

Coherent Raman and infrared spectroscopy of HCN complexes in free jet expansions and in equilibrium samples

M. Maroncelli, G. A. Hopkins, J. W. Nibler, and T. R. Dyke

Citation: *The Journal of Chemical Physics* **83**, 2129 (1985); doi: 10.1063/1.449303

View online: <http://dx.doi.org/10.1063/1.449303>

View Table of Contents: <http://scitation.aip.org/content/aip/journal/jcp/83/5?ver=pdfcov>

Published by the [AIP Publishing](#)

Articles you may be interested in

[Detection of Molecular Complex Formation and Direct Determination of Intermolecular Interaction Geometries by a Hybrid RamanInfrared Multidimensional Coherent Spectroscopy: Implications for High Throughput Biology](#)

AIP Conf. Proc. **1267**, 113 (2010); 10.1063/1.3482345

[Flowing liquid sample jet for resonance Raman and ultrafast optical spectroscopy](#)

Rev. Sci. Instrum. **74**, 4958 (2003); 10.1063/1.1614874

[Free jet infrared spectroscopy of SiF₄rare gas complexes](#)

J. Chem. Phys. **103**, 3960 (1995); 10.1063/1.469583

[Free jet spectroscopy by coherent Raman methods](#)

AIP Conf. Proc. **146**, 255 (1986); 10.1063/1.35764

[Infrared laser spectroscopy of molecular beams using a roomtemperature beam detector: Application to the study of translational freezing in freejet expansions](#)

Rev. Sci. Instrum. **53**, 1719 (1982); 10.1063/1.1136876



Coherent Raman and infrared spectroscopy of HCN complexes in free jet expansions and in equilibrium samples

M. Maroncelli,^{a)} G. A. Hopkins, and J. W. Nibler
Department of Chemistry, Oregon State University, Corvallis, Oregon 97330

T. R. Dyke
University of Oregon, Eugene, Oregon 97403

(Received 6 March 1985; accepted 20 May 1985)

Small hydrogen bonded complexes of HCN and DCN have been examined in the gas phase using FTIR and photoacoustic Raman spectroscopy (PARS). Four distinct bands are seen and assigned to CN stretching modes of the HCN dimer (D) and trimer (T). Previous microwave studies have shown the HCN dimer to be linear and analysis of the IR trimer band shape unambiguously demonstrates that the HCN trimer is also linear. The pressure dependent intensity of the observed transitions yields IR and Raman cross sections relative to the monomer of: $(\sigma_D/\sigma_M)_{\text{IR}} = 30 \pm 10$, $(\sigma_T/\sigma_M)_{\text{IR}} = 500 \pm 200$, $(\sigma_D/\sigma_M)_{\text{Ram}} = 0.5 \pm 0.1$, $(\sigma_T/\sigma_M)_{\text{Ram}} = 3.3 \pm 0.7$. The dramatic enhancements seen in the IR cross sections are due to small but significant ($\sim 2\times$) changes in the CH bond dipole derivative. CARS spectroscopy has been used to examine the complexes formed in supersonic expansions of pure HCN (DCN) and HCN diluted in Ar and He carriers. Due to the cooling and collision-free conditions in the jet, this method yields higher effective resolution than is possible with equilibrium samples. The added ability to "tune" the size of complexes by varying expansion conditions has allowed us to observe a number of other modes in HCN and DCN dimer and trimer as well as in higher polymers. These data have been used to partially refine a harmonic valence force field for the stretching modes of the dimer and trimer complexes.

I. INTRODUCTION

Hydrogen bonding plays a critical role in many chemical and biological processes and has therefore been a subject of lasting interest to chemists.¹ Among the methods used to study hydrogen bonding, gas phase spectroscopy of small A-H...B complexes has been the most successful in determining the nature of the potential energy surface upon which the hydrogen atom moves. In particular, the recent marriage of microwave spectroscopy and supersonic expansion techniques has yielded rotational data which locate the *minimum* of the potential surface and provide information concerning charge distributions in a variety of hydrogen bonded complexes.^{2,3} In favorable cases, centrifugal distortion constants and hot band intensities determined from microwave studies also allow for crude estimates of vibrational frequencies. These vibrational data are necessary if one is to develop a more accurate representation of the *shape* of the potential surface. However very few direct measurements of such values have been made for complexes in the gas phase.

Infrared vibrational spectroscopy has long been one of the classical methods used to study hydrogen bonding and an enormous literature concerning condensed phases exists.¹ Unfortunately, such studies are of limited quantitative value in defining the potential energy function since the perturbations caused by solvation and aggregation are nonnegligible compared to the hydrogen bonding interaction itself.

Most gas phase vibrational investigations have been limited to room temperature infrared measurements of the high frequency A-H stretching modes. These transitions

tend to be very broad, sometimes exhibiting substructure whose analysis can yield information about the low frequency hydrogen bond vibrations.⁴⁻⁶ Due to interference from the rotational structure of the monomer absorptions, only fairly strong hydrogen bonds, whose A-H frequencies are appreciably shifted from the monomer, can be easily studied. Much more detail is available from the spectrum if the linewidths and extent of monomer rotational structure are reduced by cooling.

Using tunable IR lasers and a cold White cell, Pine and co-workers have succeeded in obtaining rotationally resolved spectra of the HF⁷ and HCl dimers.⁸ Very recently, tunable IR laser absorption studies of supersonic expansions have yielded rotationally resolved spectra for van der Waals complexes of inert gases bound to OCS and N₂O.⁹ Similar data for other complexes is becoming available from IR vibrational predissociation spectroscopy (IVPS)^{10,11} and electric resonance techniques.¹² In contrast to the sharp line spectra (0.1-1 GHz widths) frequently observed in these experiments, linewidths of a few wave numbers have been observed for IVPS experiments with CH₃OH and NH₃ dimers¹³ and attributed to a homogeneous broadening mechanism. The vibrational relaxation and predissociation processes leading to this diversity of behavior are not well understood and are currently the subject of considerable theoretical and experimental effort.

Raman spectra of hydrogen bonded complexes can provide vibrational detail complementary to that obtained by infrared methods. In a recent paper,¹⁴ we demonstrated the first use of coherent anti-Stokes Raman spectroscopy (CARS) for obtaining such spectra of hydrogen bonded molecules in supersonic expansions. This technique is especially attractive since the wide tunability of the visible lasers employed provides access to most of the vibrational region, per-

^{a)} Current address: Department of Chemistry, 5735 S. Ellis Avenue, The University of Chicago, Chicago, Illinois 60637.

haps even the low frequency hydrogen bond stretching and bending regime. In the present paper, we report the results of CARS studies of HCN under supersonic expansion conditions. In addition, FTIR and photoacoustic Raman (PARS) spectra of equilibrium (static) samples have been obtained and give further details on the extent of HCN aggregate formation and the properties of the dimer and trimer forms.

HCN was chosen for this initial study because of the relative simplicity of linear molecule spectra and because of its high vapor pressure. In addition, some aspects of gas-phase hydrogen bonding in HCN are well known. In 1939, Giauque and Ruehrwein¹⁵ analyzed vapor density data to obtain the enthalpy and entropy of formation of the HCN dimer: $\Delta H_D = -3.28$ kcal/mol and $\Delta S_D = -16.5$ eu, indicating a weak-to-moderate strength hydrogen bond in this species. These authors also demonstrated the presence of small amounts of trimer under room temperature saturation conditions and measured its formation constants: $\Delta H_T = -8.72$ kcal/mol and $\Delta S_T = -38$ eu. The rotational spectra of the HCN dimer and its isotopic derivatives have been studied extensively.¹⁶⁻²⁰ The dimer has been shown to have a simple linear structure characterized by a hydrogen bond length $R_{HB} = 2.22$ Å¹⁸ and a dipole moment of 6.5 D.¹⁷ From centrifugal distortion constants, the hydrogen bond stretching force constant has been estimated to be 11 N/m.¹⁸ No observation of the trimer rotational spectrum has been published.

Although infrared²¹⁻²³ and even far-infrared^{23,24} spectra have been reported for HCN complexes in cryogenic matrices, the frequency variations with matrix material are substantial and the effect of the medium is difficult to judge. The only datum available for the gas phase is a single infrared dimer band observed in the CN stretching region of HCN.²⁵⁻²⁸ The bending and CH stretching modes are appar-

ently buried in the broad, intense monomer *P*, *R* branches. As far as we are aware, no Raman studies of HCN complex formation have been previously attempted.

In the work reported here, both coherent Raman and infrared methods were used to examine the high frequency vibrations of HCN (and DCN) complexes in the gas phase. A detailed analysis of an infrared band in the CN stretching region has enabled us to extract IR rotational contours of both dimer and trimer modes. Comparison of the latter with calculated contours establishes the geometry of the HCN trimer. From CARS spectra of supersonic expansions, we have determined the frequencies of other vibrations of HCN and DCN dimer and trimer. From this information a partial refinement is made of the harmonic force field for the stretching vibrations of these complexes.

II. EXPERIMENTAL

HCN was prepared by dropwise addition of concentrated H_2SO_4 onto NaCN mixed with $\sim 30\%$ H_2O (to prevent foaming). The HCN was dried by vacuum distillation through a P_2O_5 column. DCN was prepared in a similar manner using conc. D_2SO_4 (Aldrich, 98 atom % D) and D_2O (99.7 atom % D). Based on the Raman spectrum of the liquid we estimate that $\sim 5\%$ HCN impurity was present in the DCN sample.

Infrared spectra were recorded with a Mattson Instruments model "Sirius 100" FTIR. Depending on the spectral region of interest, sample cells with pathlengths between 0.5–20 cm were used. Both NaCl and KBr windows were used on these cells, with frequent cleaning being necessary at higher pressures. Scanning conditions were chosen to provide either 0.13 or 0.5 cm^{-1} resolution. Sample pressures in the infrared as well as the PARS experiments were measured with a Validyne diaphragm gauge.

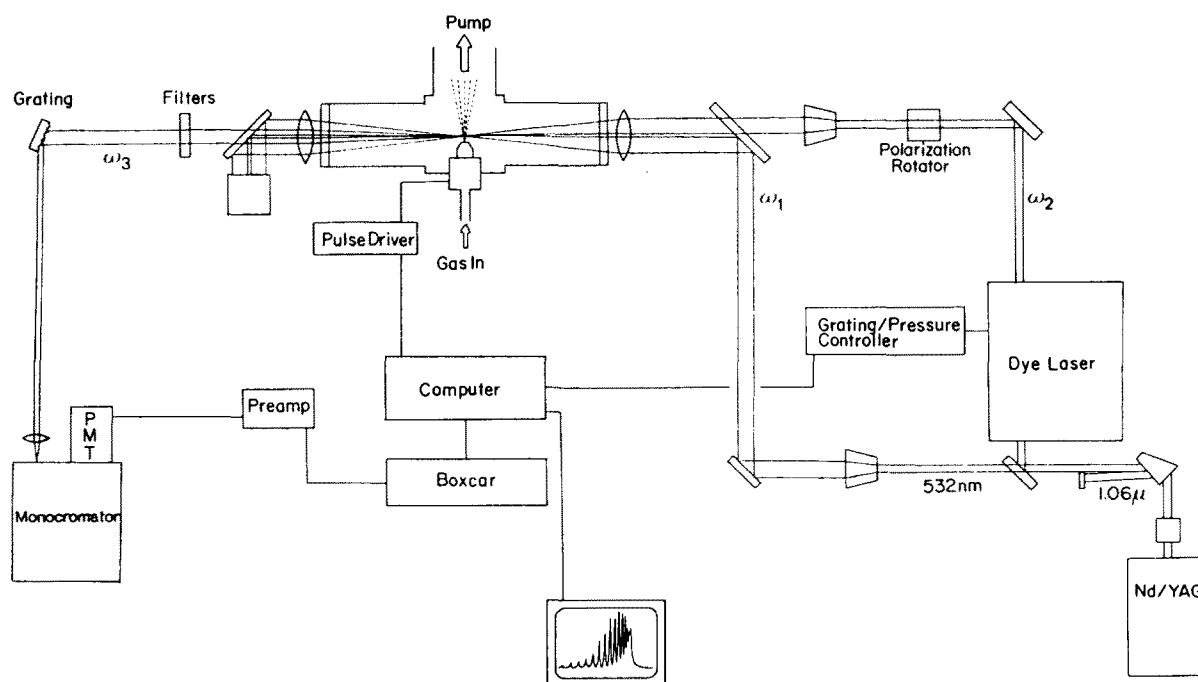


FIG. 1. Schematic diagram of the CARS/supersonic expansion apparatus.

The experimental arrangement used for recording PARS and CARS spectra has been described elsewhere¹⁴ so we give only a brief discussion here. For both measurements a Nd:YAG laser (Quanta-Ray DCR-1A) provided the 532 nm pump beam (ω_1) and a YAG-pumped dye laser (Quanta-Ray PDL-1) provided the tunable Stokes beam (ω_2). The latter could be scanned at low resolution (0.3 cm^{-1}) by stepping a grating or at high resolution (0.05 cm^{-1}) by inserting an intracavity etalon and pressure scanning the cavity. For determining Raman shifts, relative frequency calibrations were made using 0.25 and 1 cm^{-1} etalons while HCN monomer lines served as absolute frequency markers.

A schematic of the CARS layout is shown in Fig. 1. To reduce nonresonant background signal, the pump and Stokes beams were spatially separated and focused with a 300 mm fl lens at a crossing angle of $\sim 1^\circ$ at the jet position. The pulsed nozzles used in these experiments were made from fuel injector valves as described in Ref. 14. Nozzle diameters of 0.1–0.25 mm and pulse durations 0.6–1.0 ms were employed. After the jet chamber, the beams were recollimated and the CARS signal was isolated with a dichroic mirror and one or more optical glass filters. It was then sent into a 0.3 m McPherson monochromator for final rejection of the 532 light. The signal was detected with an RCA 31032 photomultiplier and the output was amplified $10\times$ with a Comlinear Corp. CLC 100 video amplifier.

For the PARS experiments, the expansion chamber (Fig. 1) was replaced by a 10 cm photoacoustic cell^{14,29} and the pump and Stokes beams propagated collinearly. The acoustic signal was detected by a Knowles model BT-1759 microphone and then filtered and amplified by an Ithaco model 2101 preamplifier.

After initial preamplification, the data collection and signal processing were the same in the PARS and CARS experiments. The respective signals were filtered, time-gated, and further amplified by a Stanford Research model SR-250 gated integrator. The output was then digitized, averaged for 10–50 shots, and stored on a DEC Micro-11 computer. Scanning of the dye laser in both high and low resolution modes was also computer controlled.

III. RESULTS

A. PARS and FTIR results with static samples

In the studies of equilibrium samples, Raman and IR spectra were recorded of room temperature HCN and DCN at pressures of 10–650 Torr. A careful search was made for features showing a different pressure dependence than the known monomer transitions.³⁰ In the FTIR experiments, the entire spectral range 400–4000 cm^{-1} was surveyed while for the PARS experiments only by the regions about ν_1 (CN stretch) and ν_3 (CH, CD stretch) of HCN and DCN were examined. In both experiments, peaks attributable to complexes were found only in the ν_1 CN stretching region of HCN.

1. Spectra

The Raman and IR spectra of HCN in the ν_1 region are shown in Figs. 2 and 3. Displayed at the bottom of each figure is a spectrum recorded at low pressure where mon-

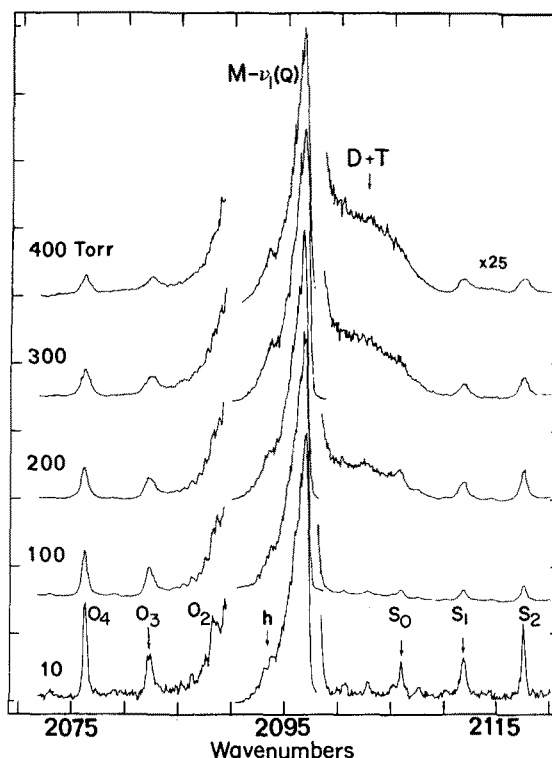


FIG. 2. Photoacoustic Raman spectra of the ν_1 region of HCN at a series of pressures. The band at 2093 cm^{-1} labeled h is the Q branch of the monomer $11^10_4-01^10_0$ hot band. D + T denotes the broad shoulder at $\sim 2103 \text{ cm}^{-1}$ assigned to unresolved dimer and trimer bands. Note the $25\times$ scale change. (The series of small peaks visible near the S branch lines in the 10 Torr spectrum are due to photoacoustic signal generated from overtone absorption of the dye laser and are P branch lines of the 20^04-000 transition.)

omer features predominate and are assigned as in Refs. 31 and 32. The remaining spectra in each figure demonstrate the growth of bands of complexes as the pressure is increased.

The PARS spectra (Fig. 2) reveal several monomer bands: an intense ν_1 Q branch, a shoulder at 2093 cm^{-1} (labeled "h") assigned as the $\nu_1 + \nu_2 - \nu_2$ hot-band Q branch, and, at $25\times$ scale expansion, much weaker ν_1 O and S branch lines. As the pressure is raised, two changes are apparent. First, the monomer lines broaden, at a rate of $1.8 \text{ cm}^{-1} \text{ atm}^{-1}$ for O and S lines of low J. This pronounced collisional broadening is due to the large dipole moment of HCN (2.95 D). We note that this pressure broadening would be expected to be even greater for the dimer with its moment of 6.5 D.¹⁷ The second feature observed as a function of pressure is the growth of a broad shoulder at $\sim 2102 \text{ cm}^{-1}$, labeled "D + T". Based on its pressure dependence, to be discussed shortly, we attribute this shoulder to a superposition of Q branches of dimer and trimer CN vibrations, slightly blue shifted from the monomer position.

The ν_1 region of the infrared spectrum shown in Fig. 3 is rather different from the Raman case. Due to a fortuitous cancellation of large CH and CN bond dipole derivatives in the ν_1 mode of HCN, this fundamental is very weak in the infrared ($\sim 1/300$ that of ν_3). As shown in Fig. 3, the $3\nu_2$ overtone ($03^10 \leftarrow 000$) and even its hot bands labeled h have intensity comparable to the ν_1 fundamental. With increasing

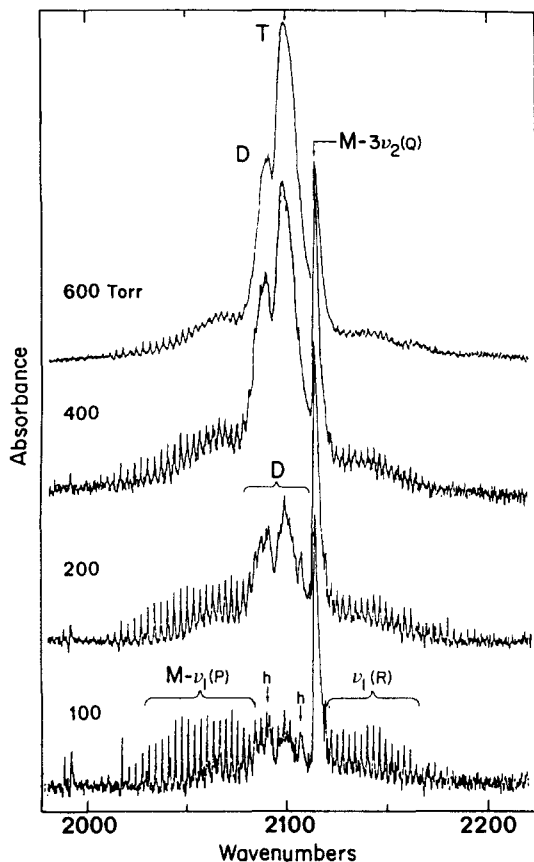


FIG. 3. Infrared spectra of the ν_1 region of HCN at a series of pressures. In addition to the P and R branch lines of the ν_1 fundamental, monomer Q branch absorptions due to $3\nu_2$ ($03^1_0 \leftarrow 000$) and its hot bands labeled h ($04^0_0 \leftarrow 01^1_0$ at 2091 and $04^2_0 \leftarrow 01^1_0$ at 2106 cm^{-1}) are also present in this spectral region (Ref. 34). Bands due to HCN complex formation are labeled D = dimer and T = trimer.

pressure, the monomer P and R lines broaden at a rate comparable to the Raman O and S lines. In contrast to the PARS spectra, at higher pressures features due to complexes are predominant in the infrared. Here the slight charge redistributions and normal mode changes accompanying complex formation greatly enhance the infrared intensities of complexes relative to the monomer, making their features easily seen over the monomer lines. The shape of the doublet for the complex at 200 Torr is approximately what is expected for an unresolved P,R contour of the linear HCN dimer. With increasing pressure however, the high frequency component (" R ") of this feature becomes relatively more intense, suggesting the formation of trimer (T ; ~ 2100 cm^{-1}). This interpretation is supported by more quantitative considerations.

2. Quantitative pressure dependence

To assign the observed ν_1 features to specific species, the relative intensities (integrated areas) of complex and monomer bands were measured as a function of pressure. For the PARS spectra the quantity determined was the ratio R_{RAM} of intensities of the complex shoulder to the monomer $\nu_1 Q$ branch. For the infrared spectra we used the ratio of the entire complex band to the monomer $3\nu_2 Q$ branch and

scaled the latter to the integrated monomer ν_1 intensity. The experimental ratios $R = S/S_M$ obtained in this manner are shown as the points plotted in Figs. 4 and 5. Inspection of either set of data shows a nonlinear pressure dependence of the relative complex-to-monomer ratio, indicating that aggregates larger than dimer contribute to these spectra. That these aggregates were formed in the gas phase, rather than as surface films on the windows, was confirmed by variation of the cell length and window material.

The composition of HCN vapor has been previously analyzed by Giauque and Ruehrwein¹⁵ who used P, V, T data to deduce equilibrium constants for dimer and trimer formation:

$$K_D = \frac{P_D}{P_M^2} = 0.0678 \text{ atm}^{-1},$$

$$K_T = \frac{P_T}{P_M^3} = 0.0152 \text{ atm}^{-2} \text{ at } 293 \text{ K}.$$

These values can be used to calculate dimer and trimer concentrations at a given total pressure. The resultant concentrations of HCN complexes are small—even at the saturation pressure (~ 650 Torr), we expect only 5.3% dimer and 0.9% trimer. From estimated equilibrium constants for higher polymers,¹⁵ we calculate less than 1% of the HCN to be contained in all higher aggregates. Neglecting the latter, our observed intensity ratios, R , are related to dimer and trimer concentrations by

$$R = \frac{S_D}{S_M} + \frac{S_T}{S_M} = \frac{\sigma_D P_D}{\sigma_M P_M} + \frac{\sigma_T P_T}{\sigma_M P_M}. \quad (1)$$

Here S is the (IR or Raman) signal and σ is the corresponding cross section. The vapor composition can be calculated as a function of pressure from K_D and K_T and the observed intensity data then fit to obtain relative cross sections.

The results of such an analysis are plotted along with the experimental data in Figs. 4 and 5. In these figures the solid

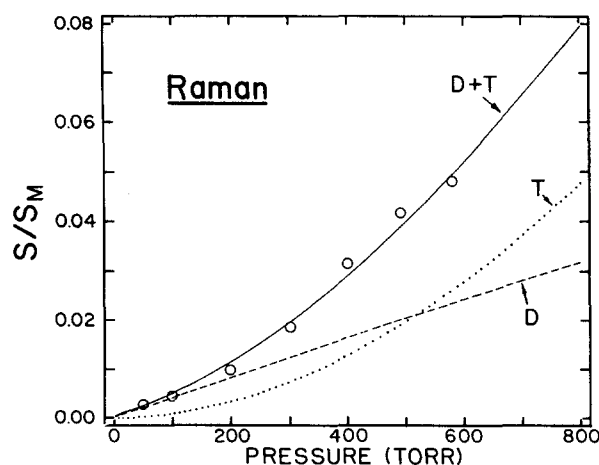


FIG. 4. Complex-to-monomer Raman signal ratios in the ν_1 region as a function of pressure. The data points are the observed ratio of the total intensity of the 2102 cm^{-1} shoulder (due to dimer and trimer) to the monomer Q branch intensity—i.e., $(S_D + S_T)/S_M$. The solid curve is the best fit to this data using Eq. (1) and dimer and trimer concentrations determined from PVT data (Ref. 15). The dashed and dotted curves show the individual signal contributions due to dimer and trimer, respectively.

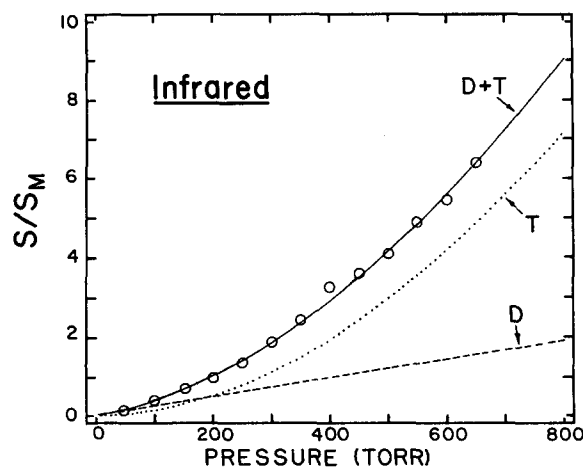


FIG. 5. Complex-to-monomer infrared signal ratios in the ν_1 region as a function of pressure. The labeling is as in Fig. 4. Due to uncertainties involved in measuring the monomer ν_1 intensity, there is an uncertainty of $\pm 30\%$ in the overall vertical scale factor even though the relative precision among points (determined with respect to the $3\nu_2$ Q branch) is much higher.

line shows the fit to the total intensity and the broken lines the separate contributions of the dimer and trimer. The quality of these fits is good, indicating that neglect of higher aggregates is reasonable. It is seen that the trimer contributes heavily in both the IR and Raman spectra, despite the fact that $P_D/P_T > 5$ even at 600 Torr. For example, at pressures higher than 400 Torr, the trimer dominates the infrared spectrum. We note that previous authors^{25–28} have erroneously attributed the infrared ν_1 complex band solely to dimeric HCN. Thus, Mettee²⁵ and Jones *et al.*²⁶ have used the temperature dependence of the intensity of this band to calculate the enthalpy of formation of the HCN dimer. The fact that the values obtained were approximately twice that determined from vapor pressure measurements¹⁵ merely reflects the fact that this band is due largely to HCN trimer under the conditions used.

The relative cross sections estimated from the above analysis are³⁴

$$\text{IR: } \sigma_D/\sigma_M = 30 \pm 10, \quad \sigma_T/\sigma_M = 500 \pm 200,$$

$$\text{Raman: } \sigma_D/\sigma_M = 0.5 \pm 0.1, \quad \sigma_T/\sigma_M = 3.3 \pm 0.7.$$

Consider the infrared case first. The large enhancement of the infrared cross sections upon complexation is a consequence of the anomalously low intensity of the CN stretch of the monomer. These increases could arise from changes in either the normal mode mix or the charge distributions as hydrogen bond formation occurs. It is well known that it is the latter effect that causes the characteristic infrared enhancement of A–H stretching modes in hydrogen bonded complexes. As will be discussed in more detail later, normal coordinate calculation show that charge redistribution is the dominant intensity-enhancing factor in these CN modes as well. The extremely large enhancement of the trimer intensity indicates that even greater electron migration occurs when this species forms.

The CN stretch has a normal Raman intensity in the monomer and it is not surprising that there is little change in the Raman cross section when complexes are formed. The

threefold increase observed for the trimer is reasonable and is supported by the normal coordinate calculations. The decrease seen for the dimer suggests that a significant part of the CN intensity may be carried by the other CN mode, seen in the IR but hidden under the strong monomer band in the Raman spectrum. We return to a consideration of the positions and intensities of these various vibrational modes as part of a discussion of the force field calculations.

3. IR band contours and trimer geometry

Although we do not resolve rotational structure, the overall band contours in the infrared spectra provide information about the dimer and trimer geometries. To determine these band shapes it was necessary to remove the interference from monomer lines, a severe problem at low pressures. Initially attempts were made to subtract out monomer spectra synthesized from the known spectroscopic constants of HCN. This approach proved unsatisfactory due to the unusual J intensity distribution within ν_1 ³² which cannot be calculated on the basis of the usual line-strength formulae. As an alternative, we used for the monomer subtraction an experimental spectrum recorded at 50 Torr, where little contribution is expected from dimer or trimer. To simulate the effects of pressure broadening, this experimental spectrum was convoluted with a Lorentzian line shape, the width of which was varied along with an intensity factor to achieve the best cancellation of monomer features at a given

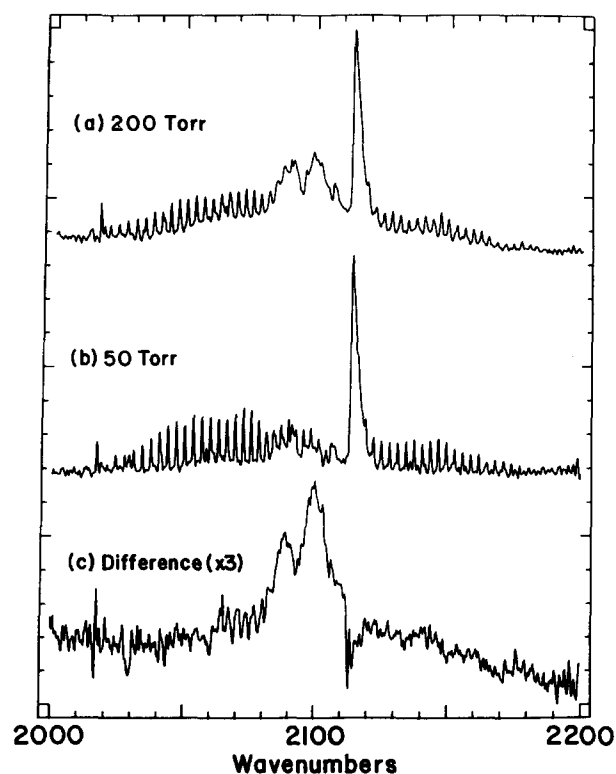


FIG. 6. Infrared spectra in the ν_1 region illustrating the method of monomer subtraction. At 50 Torr, complexes contribute very little to the observed spectrum—the apparent intensity buildup near 2100 cm^{-1} is mainly due to overlapping monomer lines. The “monomer-free” spectrum (c) was obtained by convoluting (b) with a 0.7 cm^{-1} FWHH Lorentzian line shape (to simulate pressure broadening) and subtracting (b) from (a) to give the best cancellation of monomer features.

pressure. An example of the method is illustrated in Fig. 6 for the case of a 200 Torr spectrum. As is evident from this figure, the cancellation is not perfect due to experimental noise and the fact that the pressure broadening is not identical for all lines. However, the "monomer free" spectra so obtained yield the truest representation of the band shapes of the complexes and thus are used in the calculations discussed below.

The ground state structure of the HCN dimer has been well determined by microwave spectroscopy. Based on the known value of the rotational constant¹⁸ $B_0 = 0.05823 \text{ cm}^{-1}$, we expect the dimer band shape to consist of a *P,R* doublet with peak separation of 10.0 cm^{-1} . This is indeed observed, as illustrated by Fig. 7. In the limit of low pressures, the dimer contributes most of the spectral intensity and we find a band center of $\nu_0 = 2094.7 \pm 0.5 \text{ cm}^{-1}$ for the dimer.

The change in the rotational constant with vibrational state, $\alpha = B_1 - B_0$, defines the relative heights and widths of the *P* and *R* branches and can in principle be determined from the observed spectra. Even at 150 Torr, however, there is nonnegligible trimer contribution which limits the accuracy with which this can be accomplished. Extrapolating the data to zero pressure gives a limiting *R/P* branch peak height ratio of 1.2 ± 0.2 which yields a value of $\alpha = +0.00014 \pm 0.00014$ ($\alpha/B = +0.25\%$). The band shape calculated for this α value is superimposed on the 150 Torr

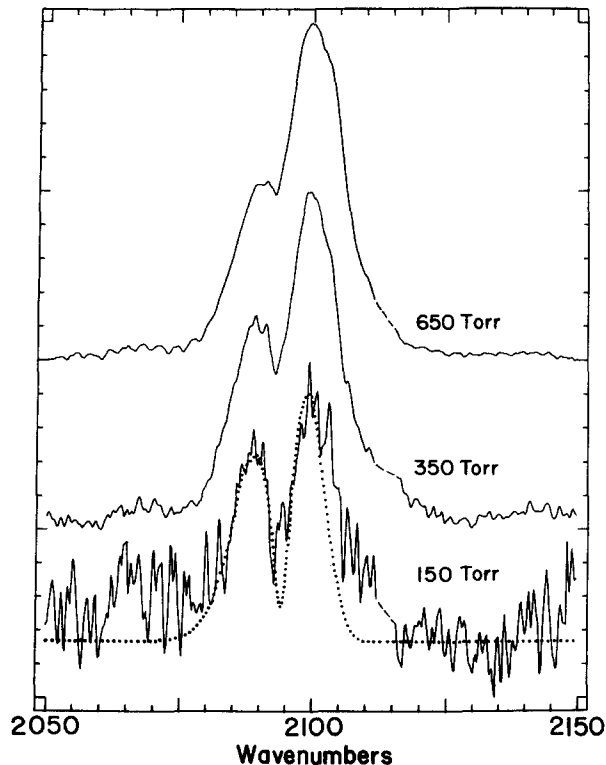


FIG. 7. Infrared spectra (after monomer subtraction) of the HCN dimer + trimer ν_1 band at three pressures. The dotted curve superimposed on the 150 Torr spectrum is the dimer band shape calculated from the constants $\nu_0 = 2094.7$, $B_0 = 0.05823$, and $\alpha = +0.00014 \text{ cm}^{-1}$ and assuming individual linewidths of 0.5 cm^{-1} .

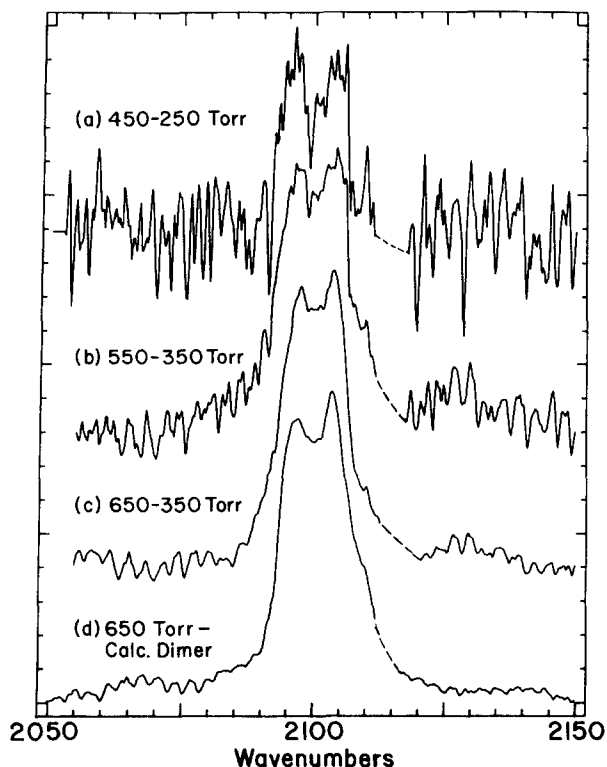


FIG. 8. Infrared spectra of the HCN trimer ν_1 band. Spectra (a)–(c) were obtained by subtracting (see the text) two experimental spectra recorded at the indicated pressures. Spectrum (d) was obtained by subtracting the dimer band calculated as in Fig. 7 from a 650 Torr experimental spectrum.

Torr spectrum in Fig. 7. We note that for the A–H stretching modes of hydrogen bonded molecules, A–H...B, an "anomalous" negative value of α is usually observed.^{7,8,35,36} This behavior has been attributed to a shortening (strengthening) of the hydrogen bond when the A–H bond lengthens due to vibrational excitation.³⁶ In the present case, α is positive and of the magnitude expected for excitation (elongation) of either CN bond by about 0.01 \AA . Such an extension is comparable to the $\sim 0.005 \text{ \AA}$ value observed for the ν_1 mode in monomeric HCN.

The band shape of the HCN trimer mode can be deduced from the higher pressure spectra by further subtraction. As noted earlier, with increasing pressure, the *R* branch component of the complex band becomes more intense relative to the *P* branch. Since the height ratio *R/P* increases continuously with pressure, we assume that the *P* component is due to dimer only. Thus, when subtracting two spectra with different dimer/trimer ratios, we use the zeroing of this low frequency peak as a test for removal of dimer. Trimer spectra generated by such subtractions are shown in Fig. 8. Traces (a)–(c) were obtained by subtracting two experimental spectra taken at the indicated pressures. To within the noise limits these spectra all show the same, nearly symmetric doublet. An identical band shape is obtained when, instead of using two experimental spectra, the calculated dimer band (as shown in Fig. 7) is subtracted from a high pressure experimental spectrum [Fig. 8(d)]. Thus we are confident that the trimer band shape can be characterized by

a central frequency of $2100.2 \pm 0.5 \text{ cm}^{-1}$, a doublet separation of $6.6 \pm 0.2 \text{ cm}^{-1}$, and a width of $14.3 \pm 0.5 \text{ cm}^{-1}$ (FWHM at $P \sim 500 \text{ Torr}$).

The gross structure of the trimer can be deduced by comparing the observed band shape with those calculated for various models. We considered four plausible structures: three cyclic and a linear trimer, illustrated in Figs. 9 and 10. The spectral band shapes also shown in these figures were calculated for these structures assuming unchanged monomer bond lengths and an H...N separation equal to that observed for the dimer (2.223 \AA^{18}). For the cyclic structures (C_{3h}), the infrared active modes are perpendicular bands with P, Q, R features, whereas the linear geometry has only P and R branches.

As is evident from Figs. 9(a)–9(c), the cyclic structures all yield band shapes which are *broader* than that observed experimentally. No collision broadening factor was included in generating these rotational contours but its addition would only increase this discrepancy. It is of course possible that more than one vibrational mode contributes to the trimer band, with perhaps two Q branches combining to give the observed contour. Again, the overall width must *increase* in this case. The only way to force the calculated spectrum to fit the observed band shape is to expand the cyclic structures (i.e., to increase the hydrogen bond lengths). However, to reproduce the observed spectrum the hydrogen bond length must be nearly doubled, a clearly unphysical situation.

The linear geometry, on the other hand, has a rotational envelope slightly *narrower* than that observed [Fig. 10(a)]. Of course, at the 500 Torr sample conditions, collisional broadening is substantial (1.2 cm^{-1} for the monomer). Much

greater broadening would be expected for trimer–monomer collisions in view of the huge dipole moment (9–10 D) expected for a linear trimer. If a line broadening of 4 cm^{-1} is assumed, excellent agreement with the experimental spectrum [Fig. 10(b)] is achieved.

In computing the spectra of Fig. 10 we have assumed $\alpha = 0$ for this trimer mode. Calculations indicate that the spectrum is very sensitive to α and the nearly symmetric spectrum observed implies that $|\alpha/B| < 0.2\%$. As with the dimer, this is consistent with simply a normal anharmonic expansion of the CN bonds upon vibrational excitation.

B. CARS spectra in supersonic expansions

Although a good deal of useful information was derived from spectra of equilibrium samples in the HCN ν_1 region, corresponding results could not be obtained for the other modes of HCN and DCN. The low concentrations of complexes and their spectral overlap with monomer features due to rotational congestion and pressure broadening greatly hamper studies with static samples. Many of these problems can be overcome by utilizing the nonequilibrium properties of free jet expansions. In this section we describe results of CARS studies of HCN, DCN expansions.

1. Jet characteristics

To observe HCN dimer in the jet using CARS, it was necessary to sample in the high density region within a few diameters of the nozzle ($X/D = 1\text{--}3$). Since this is a regime not commonly probed, it is useful to consider the expansion characteristics predicted here. The samples normally con-

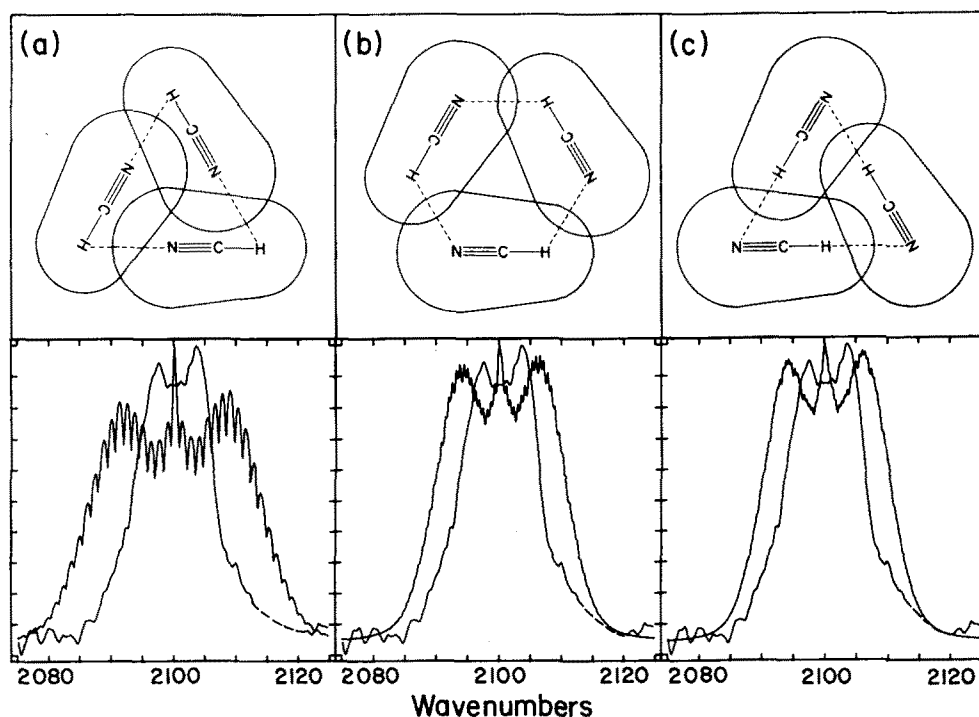


FIG. 9. Possible cyclic structures of the HCN trimer and their calculated spectra. In each spectrum of the observed trimer band is superimposed on the rotational contour calculated for the particular structure. The rotational constants used in the three simulations were: (a) $B_0 = 0.171$, (b) $B_0 = 0.095$, and (c) $B_0 = 0.088 \text{ cm}^{-1}$ (for these planar structures $A = B = 2C$). A value of $\alpha = 0$ was assumed, and an individual linewidth of 0.05 cm^{-1} was used in these computations.

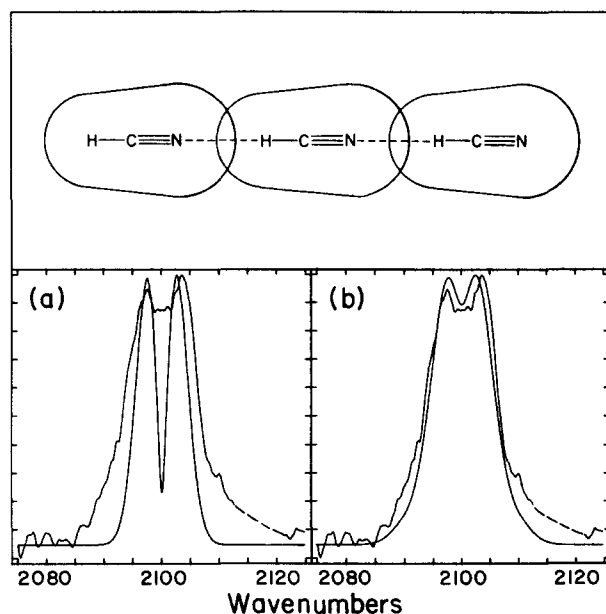


FIG. 10. The linear HCN trimer and its calculated spectrum. The observed trimer band (at ~ 500 Torr) is shown superimposed on each calculated spectrum. Both simulated spectra are based on $B_0 = 0.01532 \text{ cm}^{-1}$ and $\alpha = 0$. In case (a) an individual linewidth of 0.05 cm^{-1} was used while in case (b) a linewidth of 4 cm^{-1} was used to simulate the effect of pressure broadening.

sisted of ~ 0.6 atm of HCN, either neat or mixed with 1–5 atm of Ar, He, or N_2 carrier gas. The jet properties should be approximately those of ideal isentropic expansions with heat capacity ratios, $\gamma = C_p/C_v$, between monatomic (5/3) and linear polyatomic (7/5) values.

Figure 11(a) illustrates the relative dimensions of the expansion and laser beams employed in this work, along with translational temperature contours calculated for a pure HCN jet ($\gamma = 7/5$; $T_0 = 300$ K). Panel (b) displays the relative temperatures and densities expected for the centerline of neat HCN (dashed curves) and monatomic (solid curves) expansions. At $X/D = 1.5$, T_{tr} in the laser focal volume is about 100 K for neat HCN. For an initial HCN pressure of 0.6 atm, the HCN densities probed are equivalent to room temperature samples of 5–25 Torr, orders of magnitude higher than achievable with equilibrium samples at this temperature. The solid curves show that adding a monatomic carrier gas makes the expansion much colder ($T_{\text{tr}} \sim 50$ K) without changing the HCN density appreciably.

The degree of rotational cooling at a typical sampling point of $X/D = 1$ is revealed by the high-resolution scans of the HCN ν_1 Q branch shown in Fig. 12. Trace (a) is of a static room temperature sample at a pressure (1 Torr) such that collisional broadening is not important. Comparable linewidths are obtained in the jet [traces (b),(c)] at densities that are much higher, and the analysis of rotational structure provides a useful measure of the jet conditions. For the pure HCN jet [Fig. 12(b), $X/D = 1$], we estimate a rotational temperature $T_{\text{rot}} = 160 \pm 30$ K, reasonably close to a calculated translational value, $T_{\text{tr}} = 130$ K. Figure 12(c) confirms the additional cooling expected upon addition of argon as a driving gas; here we estimate $T_{\text{rot}} = 90 \pm 20$ K at $X/D = 1$ ($T_{\text{tr}} = 85$ K for a monatomic expansion).

2. Assignments

It is possible to alter the extent of HCN aggregation in the jet by methods to be discussed shortly. In this way the relative assignment of bands to larger or smaller size complexes is readily deduced. The specific assignment of dimer and trimer features, however, is less obvious and requires comment.

Consider the CH stretching mode. In forming a dimer, we expect the CH bond directly involved in the hydrogen bond to be significantly perturbed and we denote this as a “dimer” type bond D . The other CH bond should be little affected by hydrogen bonding and thus should retain its “monomer” character M . The dimer spectrum might thus be expected to contain one “dimer-bond” frequency significantly shifted, and one “monomer-bond” frequently nearly unshifted, from the monomer CH stretch.

In the trimer, we expect the CH bonds in the outermost HCN units to be essentially the same as in the dimer (i.e., one M and one D type bond). The central HCN unit, since it is

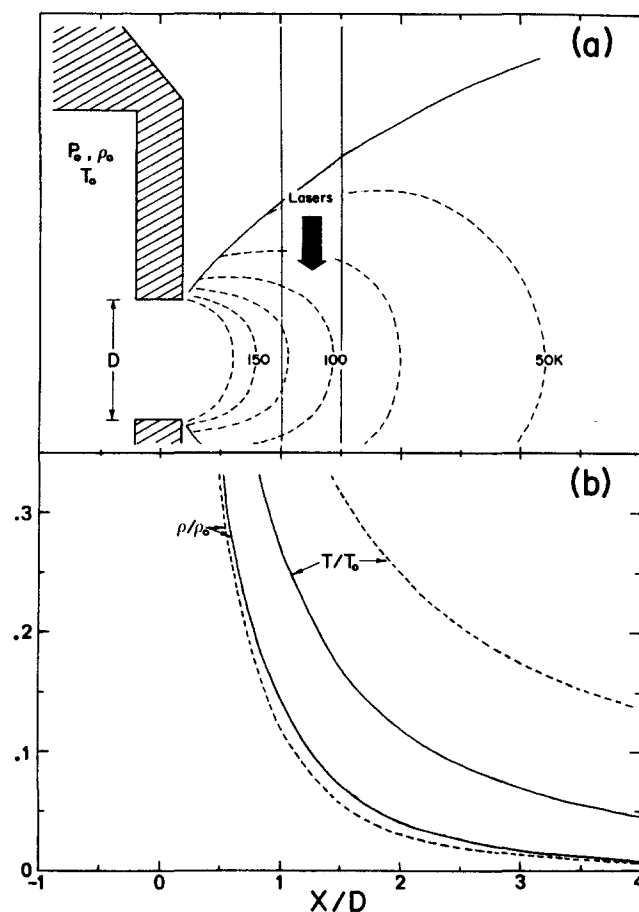


FIG. 11. Expansion conditions at the CARS sampling position. (a) Relative dimensions and positioning of the laser focus with respect to the nozzle exit. (Neither the focusing of the lasers nor their crossing is noticeable on this scale.) The dashed lines show 25 K translational temperature contours calculated for a pure HCN expansion from $T_0 = 300$ K ($\gamma = C_p/C_v = 7/5$). (b) Relative centerline temperatures (T/T_0) and densities (ρ/ρ_0) calculated for pure HCN ($\gamma = 7/5$, dashed curves) and monatomic ($\gamma = 5/3$, solid curves) expansions. Jet properties were calculated from results for ideal isentropic expansions given by Gustafson (Ref. 37).

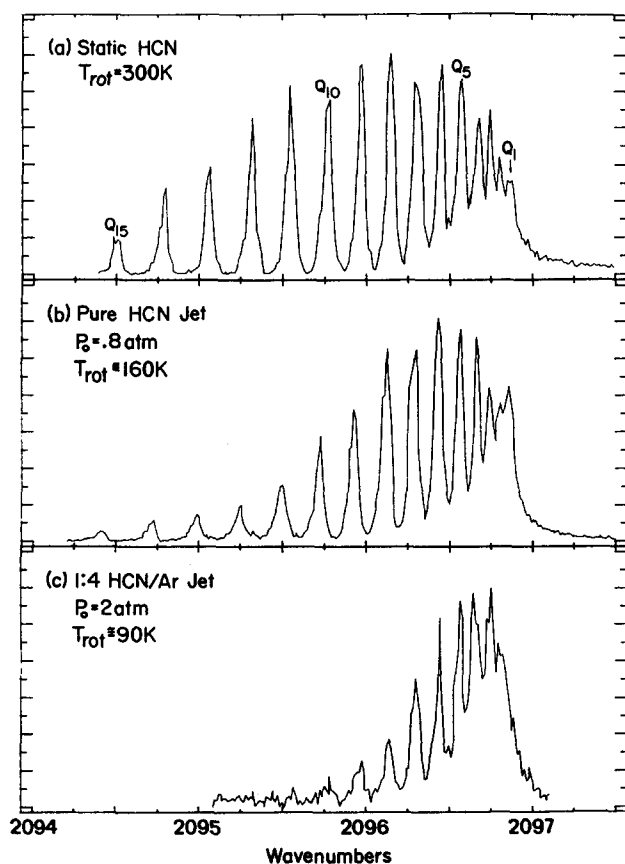


FIG. 12. High resolution (0.07 cm^{-1}) CARS spectra of the ν_1 Q branch of HCN illustrating rotational cooling at a typical sampling point in the jet. The static spectrum in (a) was taken at a pressure of 1 Torr. The jet spectra of (b) and (c) were recorded at $X/D = 1$ ($D = 0.13 \text{ mm}$). The rotational temperatures ($\pm 25 \text{ K}$) were obtained by matching the observed spectra to spectra calculated assuming a Boltzmann distribution.

hydrogen bonded to two neighbors, should be more perturbed than the D bond and we denote this new type of CH bond by T for trimer. The CH spectrum of the trimer might thus consist of three bands, probably with the frequency order: $M > D > T$.

We have shown the HCN trimer to be linear and note that the solid also consists of linear hydrogen bonded chains.³⁸ On this basis we assume linearity for all intermediate species as well. For linear n -mers with $n > 3$, we do not expect any bonds to be appreciably different than one of the three types already described. The n -mer spectrum will therefore reflect the superposition of $1M + 1D + (n - 2)T$ bonds and, for long chains, the T bond peak will dominate the spectrum.

The above picture should apply to the CN bond as well and we would thus expect the dimer and trimer to *each* give rise to *one new band* in a given spectral region (CH, CD, or CN). The formation of higher polymers should increase the intensity at the trimer frequency relative to that at the dimer frequency. While simplistic, this model does correspond reasonably well to what is actually observed. The assignment of spectral features to various bonds is also borne out by normal coordinate calculations detailed later.

3. HCN ν_1

The CARS spectra shown in Fig. 13 illustrate the features seen in the CN stretching region for pure HCN and mixed HCN/Ar expansions. These and subsequent spectra were recorded over a broad spectral range at 0.3 cm^{-1} resolution so that the HCN Q branch structure of Fig. 12 is not apparent. In the pure jet, Fig. 13(a), we observe a single symmetric peak shifted $+7.8 \text{ cm}^{-1}$ with respect to the monomer which we assign as a Q branch of the HCN dimer (D). Even at 0.07 cm^{-1} resolution, no fine structure was seen for this peak ($\text{FWHM} = 2.3 \text{ cm}^{-1}$).

Comparison of trace (a) with PARS spectra of equilibrium samples (Fig. 2) demonstrates the enhanced species discrimination provided by the decreased temperature and pressure in the jet. Assuming 0.5 for the relative dimer/monomer Raman cross sections, from this spectrum we estimate a dimer concentration of 20%, compared to 5% before expansion. Thus, in the pure HCN jet at $X/D = 1$, a fourfold increase in dimer concentration has been produced by condensation collisions during the jet expansion. A concomitant increase in trimer concentration is not expected under such mild expansion conditions. Thus, although trimer is observed in the PARS spectrum at these stagnation conditions, the quadratic density dependence of the CARS process means a 16-fold enhancement of dimer relative to trimer so that we see only the former in the jet spectrum.

The expansion conditions may be varied so as to produce more trimer as well as higher aggregates. The spectra of Figs. 13(b)–13(d) show that the addition of argon as a driving

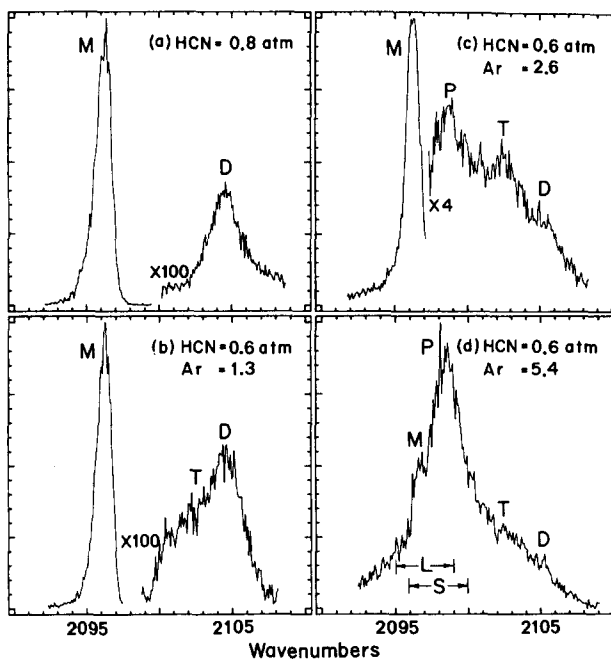


FIG. 13. CARS spectra of the ν_1 region of HCN in supersonic expansions of HCN/Ar mixtures. Peaks are labeled as M = monomer, D = dimer, T = trimer, and P = higher polymers. All spectra were recorded under similar expansion conditions ($T_0 = 300 \text{ K}$, $X/D = 1$, $D = 0.13 \text{ mm}$) except for the addition of successively higher pressures of Ar driving gas (b)–(d). In spectrum (d) the regions labeled S and L denote the position and FWHM of ν_1 in solid (78 K) and liquid (261 K) HCN (Ref.40).

gas (at constant HCN pressure) greatly increases complex formation in the jet. This results both from the lower temperatures attained with monatomic expansions [Fig. 11(b)], and from the increase in the number of three-body collisions (presumed necessary for formation of small complexes³⁹). For the 1:2 HCN:Ar mixture shown in Fig. 13(b), we observe substantially more dimer than in the pure jet. In addition, a new shoulder is observed at $+5.3\text{ cm}^{-1}$ from the monomer which is assigned to HCN trimer (T). Here the respective mole ratios are roughly $M:D:T = 25:10:1$. Thus the dimer and trimer species, which appear undifferentiated in the equilibrium PARS spectra, are readily distinguished in the jet.

Species not observable under equilibrium conditions are also easily produced in the expansions. For the 1:4 mix [Fig. 13(c)], the new peak that is observed at $+1.8\text{ cm}^{-1}$ from the monomer is attributed to higher polymers (P). In this case the total CARS signal from HCN complexes is comparable to that from the monomer. Finally, at 5.5 atm of argon [Fig. 13(d)] the spectrum is dominated by the polymer band. For comparison, in Fig. 13(d) we show the frequencies of HCN in the solid ($\sim 150\text{ K}$) and liquid ($\sim 300\text{ K}$) phases. It is interesting that the sequence of Raman active lines ($M < P < T < D$) does not fit the idea of a gradual gas to solid shift as aggregation occurs. Rather, as seen later, this ordering is a sensitive function of the normal coordinate mix.

It is important to note that the same spectral features and frequencies described above for HCN/Ar expansions were also observed with N_2 and He as driving gases. This allows us to be sure that we are indeed observing HCN complexes and not mixed HCN-carrier gas species.

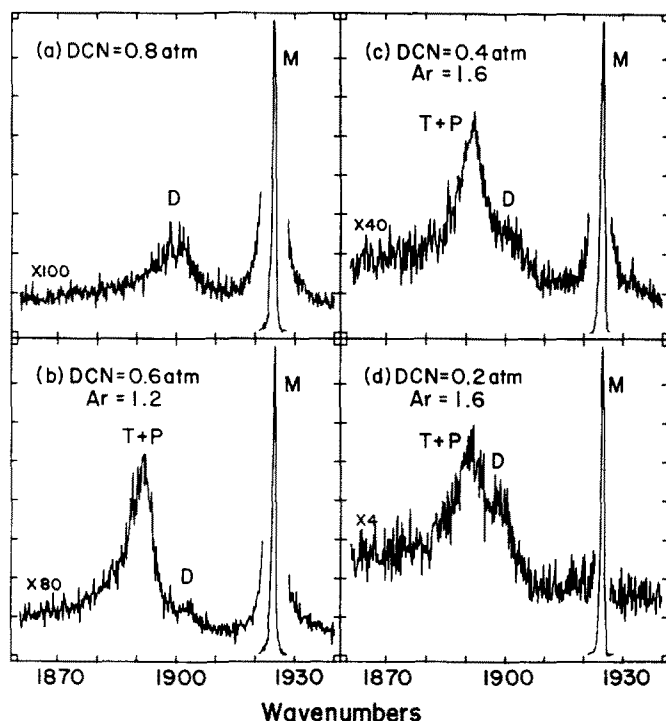


FIG. 14. CARS spectra of the ν_1 region of DCN in DCN/Ar expansions (conditions the same as in Fig. 13). The series (b)–(d) illustrate the effect of dilution with Ar at a fixed total driving pressure. Note the different gain changes in these spectra.

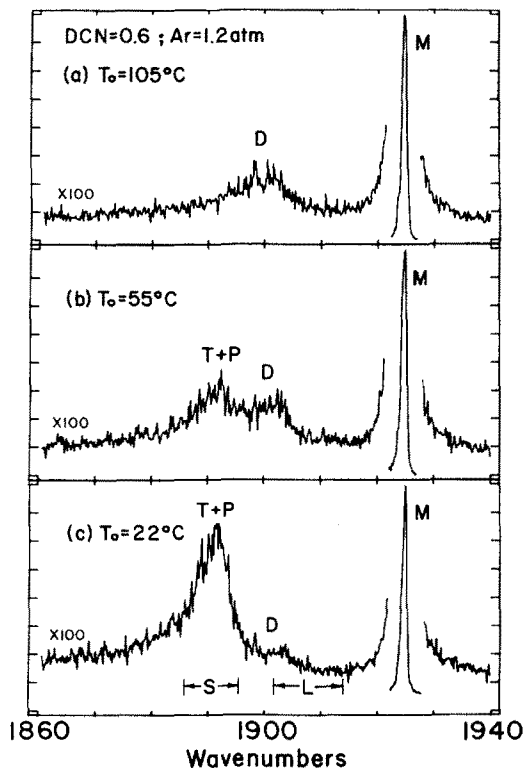


FIG. 15. CARS spectra of the ν_1 region of a 1:2 DCN/Ar expansion showing the effect of variations in the nozzle temperature T_0 . S and L show the frequencies observed for solid and liquid DCN (Ref. 40).

4. DCN ν_1

Figures 14 and 15 show spectra recorded in the ν_1 region of DCN in DCN/Ar jets and illustrate the effect that other variables have on complex formation. In the pure DCN jet of Fig. 14(a), we observe a single broad (FWHM = 11 cm^{-1}) band at -24.9 cm^{-1} with respect to the monomer. We assign this band to DCN dimer (D). As will be discussed in more detail later, the greater breadth and shift of this DCN dimer transition, as compared to that of HCN dimer, reflects greater mixing of the CN and CD coordinates in DCN.

Under conditions favoring greater complex formation, such as in Figs. 14(b)–14(d), we resolve only one additional band, at -34.9 cm^{-1} relative to the monomer (FWHM = 8 cm^{-1}), which we assign to all higher complexes including trimer ($T+P$). As for HCN, its frequency and width are similar to the corresponding band observed in solid DCN [see Fig. 15(d)].

The series of spectra in Figs. 14(b)–14(d) show the effect of dilution with argon while keeping a fixed total pressure. The initial addition of argon increases the polymer-to-dimer ratio due to the greater cooling efficiency of Ar relative to HCN. With increasing dilution, however, this trend reverses and the aggregation is less likely due to the reduced number of DCN–DCN collisions available for complex formation. Figure 15 shows that changing the nozzle temperature provides one further means for controlling the polymer/dimer ratio in these expansions. As illustrated in this series, increasing the source temperature by a few tens of degrees has a profound effect on the complexes observed, greatly inhibiting the formation of larger aggregates.

5. ν_3 HCN, DCN

Many studies have established strong correlations between hydrogen bond strength and the frequency shift, bandwidth, and IR intensity enhancement of the A–H stretching mode.¹ Unfortunately the Raman spectra do not enjoy any special intensity enhancement as the electrons redistribute, and the bandwidth increase makes the observation of these transitions difficult. The CH stretch (ν_3) in HCN is no exception. To increase the detection sensitivity in these experiments, it was necessary to reduce the nonresonant background by use of helium rather than argon as the carrier gas. Spectra of a number of mixtures are shown in Fig. 16.

Under conditions that we expect to favor the formation of large aggregates, illustrated here by Fig. 16(c), a broad band due to complexes is apparent in the ν_3 region. This

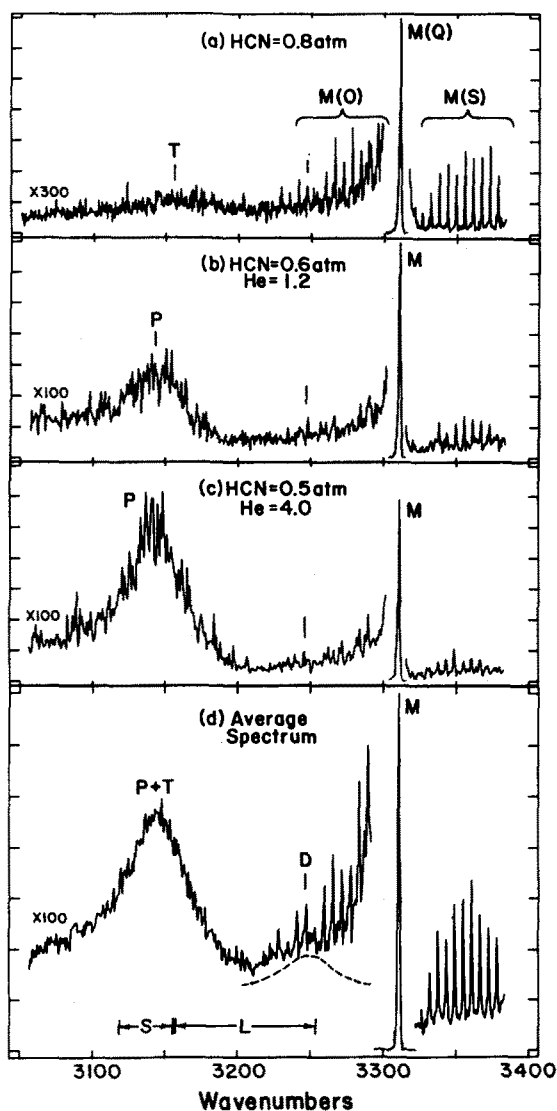


FIG. 16. CARS spectra in the ν_3 region of HCN in HCN/He expansions (conditions as in Fig. 13). Traces (a)–(c) show spectra of conditions favoring increasing degrees of aggregation. Spectrum (d) is a “composite” spectrum obtained by averaging a set of 14 spectra similar to (a)–(c). This spectrum does not correspond to any particular mixture composition and is used merely to show that a band occurs reproducibly at ~ 3250 cm^{-1} (dashed peak). *S* and *L* denote the solid and liquid state frequencies (Ref. 40).

polymer band occurs at 3144 cm^{-1} and has a FWHH = 54 cm^{-1} , very similar to what is observed in solid HCN (shown at the bottom of Fig. 16).

For expansions of pure HCN at low pressures, the ν_1 studies indicate that mainly dimer is present. Under similar conditions the ν_3 region [Fig. 16(a)] shows a broad, barely perceptible band at roughly the same shift as in the polymer. (Note the scale change here is $300\times$ compared to $100\times$ used in the ν_1 region.) Repeated scanning of this region in the pure jet shows this band reproducibly broader (FWHH = 73 ± 7 cm^{-1}) and at slightly higher frequency ($\nu_0 = 3160 \pm 6$ cm^{-1}) than the polymer band. There is evidence for one additional band occurring under the tail of the monomer *Q* branch. In an attempt to demonstrate the presence of this very weak feature, Fig. 16(d) shows a composite spectrum obtained by signal averaging 14 various scans of HCN/He mixtures similar to spectra (a)–(c). The existence of a band having roughly the position (~ 3246 cm^{-1}) and intensity shown by the dashed curve is quite reasonable, although admittedly not proven by this data. Nonetheless, the assignment of this transition as the “bound” CH stretch of the dimer is favored for various reasons to be discussed below. The 3160 cm^{-1} transition is then attributed to trimer with perhaps some contribution from higher aggregates.

No features due to complexes were seen in the corresponding ν_3 region of DCN. The Raman intensity in this case is roughly $25\times$ smaller than that of HCN and, due to the quadratic dependence of the CARS cross section, detecting even the monomer itself was difficult.

IV. DISCUSSION

A summary of the frequencies determined from the IR and CARS experiments and their assignments to specific HCN (DCN) complexes is provided in Table I. Part of the justification for our choice of assignments comes from comparing these results with observations made on similar systems and from normal coordinate calculations.

A. Comparison of HCN dimer with related compounds

Our HCN dimer results are displayed in Table II along with those previously obtained for similar systems. The mode labeling used in the following discussion is indicated in the Table II headings. Where our experiments do not determine the frequency, values deduced from normal coordinate calculations are given in parentheses. A direct comparison with gas-phase frequencies may be made only with the heterodimers formed between HCN and the bases dimethyl ether⁴³ and ammonia.²⁶ However, a number of researchers have studied HCN complexes in cryogenic matrices^{21–24,42} and Table II includes recent data of this type. The entries correspond to the shifts relative to matrix-isolated monomer for Ne, Ar, Kr, and N_2 hosts.

For the CN stretches, the shifts from the monomer value are small ($< 2\%$) and all of the data suggest that the “bound” CN1 bond stretch occurs at a frequency *higher* than that of the “free” CN2 moiety. The shifts change significantly upon deuteration and are a sensitive function of normal coordinates (*vide infra*). Qualitative agreement is seen between the gas phase and matrix results for the HCN

TABLE I. Summary of observed frequencies.^a

Frequency (cm ⁻¹)	Shift (cm ⁻¹)	FWHH (cm ⁻¹)	Method; conditions	Assignment
DCN ν_1 region				
1890.5 ± 0.5	- 34.7	7.9 ± 0.4	CARS ; 100 K	<i>T</i> (+ <i>P</i>)
1900.3 ± 0.5	- 24.9	11 ± 1	CARS ; 150 K	<i>D</i> (+ <i>T</i> ?)
1925.2	Ref. 31 ; 293 K	<i>M</i>
HCN ν_1 region				
2094.7 ± 0.3	- 2.1	18 ± 3	IR ; 293 K	<i>D</i>
2096.8	Ref. 31 ; 293 K	<i>M</i>
2098.6 ± 0.5	+ 1.8	2.8 ± 0.5	CARS ; 100 K	<i>P</i>
2100.2 ± 0.5	+ 3.4	14 ± 1	IR ; 293 K	<i>T</i>
2102.1 ± 0.5	+ 5.3	2.6 ± 0.3	CARS ; 150 K	<i>T</i>
2104.6 ± 0.3	+ 7.8	2.6 ± 0.3	CARS ; 150 K	<i>D</i>
HCN ν_3 region				
3143.9 ± 0.6	- 167.6	54 ± 4	CARS ; 100 K	<i>P</i>
3160 ± 6	- 152	73 ± 7	CARS ; 150 K	<i>T</i> (+ <i>P</i> ?)
3246 ± 15	- 65	~60	CARS ; 150 K	<i>D</i> (?)
3311.5	Ref. 31 ; 293 K	<i>M</i>

^aThe CARS frequencies and their associated errors refer to the band maxima which may differ from the actual ν_0 ($J = 0 \leftarrow J = 0$) by \pm (FWHH/2).

dimer, but it is apparent that the variation with matrix is appreciable. In other words, the matrix environment causes nearly as large a perturbation on this vibrational motion as does hydrogen bonding itself.

The free CH1 stretch in the dimer was not seen in this work and is presumed to lie under the monomer. The small shifts observed in the matrix studies support this conclusion. The bound CH2 is expected to occur at a much lower frequency however and to give a more direct measure of the hydrogen bond strength. As mentioned earlier, candidates for this vibration are two weak features seen in the gas phase CARS spectra, shifted 152 and 65 cm⁻¹ below the monomer frequency. Because of the marginal quality of the spectra in the latter region, it is helpful to seek an independent estimate of this shift.

One might expect the hydrogen bond strength, and thus the CH2 stretching frequency, to correlate with the proton affinities of bases complexed with HCN. Gas phase affinities

for HCN, OMe₂, and NH₃ are 179, 193, and 205 kcal/mol, respectively,⁴⁴ which would predict a shift for HCN dimer smaller than the - 127 and - 161 cm⁻¹ values seen in the OMe₂ and NH₃ complexes. This conclusion is supported by a comparison of microwave results for HCN...HCN and H₃N...HCN. Respective indicators such as the hydrogen bond length (2.22 vs 2.16 Å), the hydrogen bond stretching force constant (11 vs 12 N/M), and the dipole moment enhancement (0.77 vs 0.94 D) all imply that the bond is stronger in the ammonia complex.^{17,18,45} These points argue against the - 152 cm⁻¹ band being a dimer mode. In this connection, it should also be noted that an HCN dimer band shifted as much as 152 cm⁻¹ would fall outside the intense monomer *P* branch in the infrared spectrum. We found no trace of an IR band in this region and judge that a shift greater than ~ 80 cm⁻¹ should have given rise to a detectible feature if the intensity were comparable to that seen in the ammonia and ether complexes.

TABLE II. Comparison of HCN dimer-monomer shifts with those in related systems.

System	HCN[1]---HCN[2]				DCN[1]---DCN[2]				
	ν_1 region		ν_3 region		ν_1 region		ν_3 region		
	CN1	CN2	CH1	CH2	CN1	CN2	CD1	CD2	
HCN---HCN (this work)	Gas ^a	+ 7.8	- 2.1	(10.8)	- 65	(- 1.2)	- 24.9	(21.2)	(- 29.5)
HCN---HCN (Ref. 21)	Ne	+ 21.6	+ 5.7	+ 11.7	- 68.5	+ 4.5	- 11.8	+ 6.2	- 36.2
	Ar	+ 21.4	+ 3.6	- 1.3	- 101.7	+ 10.7	- 24.3	+ 5.1	- 52.3
	Kr	+ 23.6	+ 3.3	- 5.2	- 97.7	+ 9.7	- 24.6	+ 3.1	- 50.4
	N ₂	+ 13.1	- 4.9	- 5.3	- 82.7	+ 7.6	- 21.5	+ 1.1	- 41.9
HF---HCN	Ar	- 32.2	- 19.6
HCN---HF (Ref. 42)	Ar	+ 29.7	+ 16.6
Me ₂ O---HCN (Ref. 43)	Gas	...	- 11	...	- 127	...	- 10	...	- 65
H ₃ N---HCN (Ref. 26)	Gas	...	- 11	...	- 161	...	- 35	...	- 70

^a Values in parentheses are shifts calculated as described in the text.

Finally, a semiquantitative estimate of the CH shift can be obtained from the correlations shown in Fig. 17. The bottom panel shows values of N...H distances vs $\Delta\nu/\nu$ for the HA stretch in several XCN...HA gas phase complexes. This correlation and the measured hydrogen bond length for HCN dimer yield a shift of about $-60 \pm 20 \text{ cm}^{-1}$. The upper panel permits the estimate of a gas phase frequency from more easily obtained argon matrix shifts. This is a plot of $\Delta\nu/\nu(\text{Ar})$ vs $\Delta\nu/\nu(\text{gas})$ for complexes of HF and HCl with various bases.⁴⁶ Also included are data for a single base (dimethyl ether) complexed with a range of acids (ROH alcohols).⁴⁷ The quality of this simple correlation for such a range of hydrogen bonded systems indicates that the effect of the argon medium on the AH stretching motion is reasonably constant. A least squares fit indicates that the fractional shift for the gas phase is $78 \pm 15\%$ of the Ar matrix value

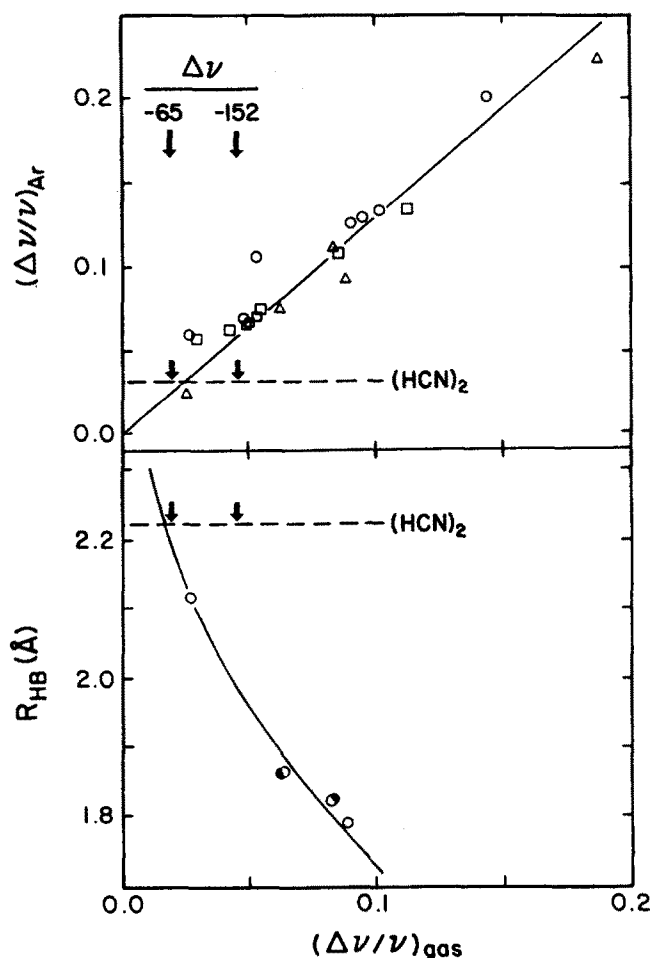


FIG. 17. Correlations of gas phase (A-H) frequency shifts with the corresponding shifts observed in argon matrices (top panel) and with hydrogen bond lengths (R_{HB} ; bottom panel). Arrows indicate the shifts (-65 and -152 cm^{-1}) of two alternatives for the CH1 assignment. Relative frequency shifts are defined as: $\Delta\nu/\nu = (\nu_{\text{monomer}} - \nu_{\text{complex}})/\nu_{\text{monomer}}$ where all frequencies refer to a single phase, either gas or Ar matrix. The data in the top panel correspond to complexes of various bases with HF (triangles) or HCl (circles) (Ref. 46) and to various alcohols with the base dimethyl ether (squares) (Ref. 47). The line is the least squares fit to this data. The data in the bottom panel are for various acids A-H in R-CN...H-A complexes and were obtained from Refs. 2, 5, and 6. R_{HB} is the N...H distance. The half-filled circles correspond to overlapping A-H and A-D data pairs. The curve is drawn here only to aid in visualization.

and this predicts a shift of $-79 \pm 15 \text{ cm}^{-1}$ for HCN dimer. Thus all the evidence is consistent with our choice of -65 cm^{-1} shift for the bound CH stretch and we assign the -152 cm^{-1} feature to trimer and perhaps higher aggregates.

B. Normal coordinate calculations

We have used the observed stretching frequencies of the HCN and DCN dimer and trimer (Table I) to partially refine a force field for the axial stretching motions in these hydrogen bonded molecules. The motivations for such calculations are: (i) to use calculated frequencies and intensities to determine whether the assignments made are reasonable, (ii) to identify modes which may have been overlooked in the experimental spectra, and (iii) to relate the observed frequency shifts to changes in the bond properties as reflected in the valence force constants. As is usually the case, we have too few experimental frequencies to fully determine the force field for the dimer and trimer. For this reason we approach the problem stepwise, considering in order the monomer, the dimer, and then the trimer, keeping some force constants in the larger molecules fixed at the values determined in the preceding calculation. Table III schematically demonstrates this procedure.

1. Monomer

We have chosen to fit harmonic frequencies for the monomer (Ref. 33) rather than observed frequencies in these refinements. If the latter are fit, the average frequency deviation is 7 cm^{-1} for HCN and DCN. Since many of the observed frequency shifts due to hydrogen bonding in the dimer and trimer are of this same magnitude, such a starting error is unacceptable. We therefore base the dimer and trimer fits on approximate harmonic frequencies instead of those actually observed. These harmonic frequencies are calculated for the complexes by adding the complex-monomer shifts to the harmonic monomer frequencies, thereby assuming the same anharmonicity for all species.

To describe the nature of the normal modes, we have indicated the most important stretching components and their relative sign in Table IV. The numbers in parenthesis refer to the diagonal potential energy distribution (PED) defined as

$$\text{PED}(R_j)_k = 100F_{jj}^2L_{jk}/\sum_i F_{ii}^2L_{ik}, \quad (2)$$

where the F_{jj} are the diagonal force constants and L_{jk} is the L -matrix element connecting bond stretch R_j with normal mode Q_k ($\mathbf{R} = \mathbf{LQ}$). The results for monomeric HCN show that the normal modes are relatively "pure" ($\sim 95\%$) CH and CN bond stretches. In DCN, due to the closer match between the CD and CN frequencies, there is a strongly mixed character to both modes.

Relative IR intensities, based on simple addition of bond dipole derivatives, were calculated as

$$I_{\text{IR}}(Q_k) \propto (\partial\mu/\partial Q_k)^2 = [\sum_j L_{jk}(\partial\mu/\partial R_j)]^2. \quad (3)$$

CH and CN dipole derivatives of 1.06 and -0.36 D/\AA were derived from the experimental results of Hyde and Hornig.^{28,48} Intensity values listed in Table IV are scaled to 100

TABLE III. Harmonic stretching force constants (N/M) for HCN complexes.^a

- 21.1					
H-C≡N					
624.4		1871			
- 34.5			- 34.5		
H-C≡N----H-C≡N					
(624.4)	1894	(11)	586.9	(1871)	
(- 34.5)			(- 34.5)		
H-C≡N----H-C≡N----H-C≡N					
(624.4)	(1894)	(11)	553.8	1896	(11) (586.9) (1871)

^aThe CH-CN interaction constant is shown above, the bond stretching constants below the structure. Values shown in parentheses were held fixed.

for the most intense monomer mode. A similar expression was used to calculate relative Raman intensities. In this case, experimental values were not available; instead, average bond polarizability derivatives of 0.851 (CH) and 2.56 Å² (CN) were obtained from the SCF calculations of Greedy *et al.*⁴⁹ The calculated Raman intensities for the monomer agree with our semiquantitative observations on the *Q* branch strengths [$\nu_1(\text{HCN}) \approx \nu_1(\text{DCN}) > \nu_3(\text{HCN}) > \nu_3(\text{DCN})$], pro-

viding reassurance that these theoretical derivatives are reasonable.

2. Dimer and trimer

For the dimer and trimer calculations we assumed that the exterior CH and CN bonds were unaffected by hydrogen bonding and fixed the force constants at the monomer values. The force constant for the hydrogen bond was set to 11

TABLE IV. Summary of normal coordinate calculations.

Harmonic frequency (cm ⁻¹)	Calculated frequency (cm ⁻¹)	Shift D-M,T-M (cm ⁻¹)	Infrared intensity (Calc.)	Raman intensity (Calc.)	Mode description (PED %)
HCN					
3441.2	3441.2	...	100	23	CH(95) - CN(5)
2128.7	2128.7	...	0.1	100	CN(94) + CH(6)
DCN					
2703.3	2703.3	...	51	1	CD(68) - CN(32)
1952.1	1952.1	...	5	91	CN(67) + CD(33)
HCN[1]---HCN[2]					
...	3452.0	+ 10.9	98	21	CH1(94)
3376.2	3376.0	- 65.1	102	22	CH2(93)
2136.5	2136.7	+ 8.0	0.3	143	CN1(89)
2126.6	2122.6	- 6.1	0.2	60	CN2(88)
...	116.3	HB(98)
DCN[1]---DCN[2]					
...	2724.5	+ 21.2	48	1	CD1(66) + CN1(33)
...	2673.8	- 29.5	53	2	CD2(63) - CN2(36)
...	1950.9	- 1.3	8	123	CN1(63) + CD1(33)
1927.2	1929.4	- 22.7	4	57	CN2(61) + CD2(35)
...	114.3	HB(98)
HCN[1]---HCN[2]---HCN[3]					
...	3452.0	+ 10.9	99	21	CH1(94)
...	3376.0	- 65.1	98	21	CH3(92)
3289.2	3289.7	- 151.4	103	20	CH2(91)
2134.0	2138.1	+ 9.4	0.6	223	CN1(64) + CN2(27)
2132.1	2131.7	+ 3.0	0.2	24	CN2(58) - CN1(29)
...	2121.5	- 7.2	0.1	59	CN3(86)
...	142.6	HB1 - HB2
...	82.2	HB1 + HB2
DCN[1]---DCN[2]---DCN[3]					
...	2724.5	+ 21.1	50	1	CD1(66) - CN1(33)
...	2673.6	- 29.7	46	2	CD3(63) - CN3(36)
...	2635.2	- 68.1	54	4	CD2(58) - CN2(41)
...	1950.6	- 1.5	8	117	CN1(64) + CD1(34)
...	1930.4	- 21.7	10	122	CN3(59) + CD3(33)
1917.4	1915.6	- 36.5	3	30	CN2(53) + CD2(38)
...	140.2	HB1 - HB2
...	80.7	HB1 + HB2

N/M, the value estimated from microwave spectroscopy using centrifugal distortion data.¹⁸ The high frequency modes proved insensitive to the particular value chosen for this constant. Four experimental frequency shifts were observed for the HCN and DCN dimers and these served to constrain the interior bond constants. The results of the calculations are summarized in Tables III and IV.

A number of force fields were considered for the dimer. A diagonal field in which only the inner CH and CN bonds were varied gave a poor fit. Including a CH–CN interaction constant, fixed at the monomer value, gave better results—an average error of $\delta = 5.5 \text{ cm}^{-1}$ for the dimer shifts. However the fit of the “free” CN stretch of the deuterated dimer was still particularly bad (error of 15 cm^{-1}). To partially account for the effect of hydrogen bonding on the terminal groups, this interaction constant was allowed to vary. A significant improvement resulted, the average error for the dimer shifts (1.6 cm^{-1}) being within our experimental uncertainty. Finally, an “exact” fit was achieved when the terminal CN bond constant was also allowed to vary. In this case however, the constants were so highly correlated and had such large uncertainties as to have little meaning. Thus the results in Tables III and IV are judged the most reasonable description of the force field of the dimer.

The trimer calculations summarized in the tables are based on the assumption that the two end HCN molecules were identical to their counterparts in the dimer. The hydrogen bonding and off-diagonal force constants were chosen as in the dimer calculation. The four observed frequencies were used to refine only the CH and CN diagonal constants for the central monomer unit. Again the frequency fit was quite good, $\delta = 1.7 \text{ cm}^{-1}$.

The normal modes calculated for the dimer and trimer (Table IV) share the following features. First, hydrogen bonding does not appreciably alter the form of the vibrations *within* the monomer subunits from that calculated for the free monomer (compare the DCN monomer and dimer PED's for example). Second, only in the HCN trimer is there significant coupling of motions in adjacent units, i.e., in the CN1 and CN2 stretches which are the closest to resonance. All other CH (CD) and CN molecular vibrations are such that the motion is mainly confined to only *one* of the monomer subunits. It should be said that some mixing with the hydrogen bond stretches is apparent in the normal coordinates but this makes a relatively small contribution to the PED of the internal stretches of each monomer. We note that the low frequency trimer vibrations consist of pure symmetric and antisymmetric combinations of the hydrogen bond stretches. These modes occur at $\pm 26\%$ of the frequency of the dimer, suggesting that an easy distinction among different aggregates may be possible in the low frequency region of the spectrum.

The normal coordinate calculations show the dimer and trimer to consist of weakly coupled monomer subunits, each with slightly different frequencies. This feature, in concert with our fixing of force constants, produces the many frequency coincidences expected from the “bond mode” picture discussed earlier. For example in the regions ν_1 and ν_3 , the calculated trimer frequencies predict a spectrum with

three bands: one masked by monomer, one by dimer, and only one shifted sufficiently to signal the presence of trimer. Similarly, calculations of frequencies of mixed deuterides such as HCN---DCN, etc. indicate that the vibrations of these species would be difficult to distinguish from those of the parent isotopic forms.

3. Intensities

Intensity calculations provide added assurance that our frequency assignments are reasonable and that no transitions have been overlooked. For this purpose we assumed that the CH and CN bond derivatives in the dimer and trimer were unchanged from their monomer values and that the hydrogen bond stretch contributed negligibly to the intensities. These approximations are probably most reasonable for the calculation of Raman cross sections. All CH stretches of the dimer and trimer are predicted to have comparable (and low) Raman intensities. These drop another order of magnitude for the CD modes, making them unobservable in our spectra.

In the dimer, the bound CN1 stretch is calculated to have the highest Raman intensity. For $(\text{HCN})_2$ this mode is indeed seen, but in $(\text{DCN})_2$ the band is predicted to fall under the strong monomer Q branch and therefore to be undetectable. The reverse behavior occurs for the weaker free CN2 stretch of the dimer isotopes. In $(\text{HCN})_3$, the observed CN Raman band is predicted to dominate the trimer spectrum, an enhancement resulting from the in-phase addition of the bound CN1 and CN2 stretching motions. The calculated cross section is 2.2 times that of the monomer, reasonably close to the 3.3 ratio deduced from the PARS intensities. This agreement may be partly fortuitous since the calculated dimer/monomer ratio (1.4) is three times larger than the experimental value of 0.5 deduced earlier. Without further experimental and theoretical investigation, all that can be said is that changes in Raman intensities and polarizability derivatives caused by hydrogen bond formation are modest. This is consistent with conclusions reached in other Raman studies of hydrogen bonding.^{50,51}

Comparison of calculated and observed infrared intensities reveals large discrepancies that are more indicative of changes induced by hydrogen bonding. This result is partially a consequence of the anomalously low intensity of the CN stretch in the monomer. Writing the dipole derivative as

$$\begin{aligned} \partial\mu/\partial Q = & (\partial\mu/\partial R_{\text{CH}})(\partial R_{\text{CH}}/\partial Q) \\ & + (\partial\mu/\partial R_{\text{CN}})(\partial R_{\text{CN}}/\partial Q), \end{aligned} \quad (4)$$

we note that the low intensity of the CN mode occurs through a fortuitous cancellation of four relatively large derivatives on the right-hand side of this expression. Small changes in any of these derivatives can produce dramatic intensity enhancements. For example, in monomeric DCN, a 50-fold increase in the CN intensity results from the change in the $\partial R/\partial Q$ terms. The normal mode changes in HCN on polymerization are much smaller however, and lead to calculated increases of only 1 to 6 (Table IV). The experimental dimer and trimer enhancements (30, 500) for the observed CN stretches are more than an order of magnitude greater. This is a clear indication of the large increase in

$\partial\mu/\partial R_{\text{AH}}$ which is known to occur in hydrogen bonded systems. Our calculations for the monomer show that a twofold increase in the CH derivative produces a factor of 30 enhancement in the infrared intensity for the CN stretch. Such an increase is quite reasonable on hydrogen bonding. Analogous derivative changes of factors of 3 to 4 have been reported in recent *ab initio* calculations on $(\text{H}_2\text{O})_2$ and $\text{HCN}\cdots\text{HF}$ and are attributed to dynamic charge transfer and polarization effects accompanying the proton movement.⁵² Similar calculations for HCN dimer and trimer species would be of some interest since the measured enhancement factors of these simple linear molecules should provide a good test of the reliability of charge flows predicted by theory.

4. Harmonic force constants

Finally, we comment on the force constant changes brought about by hydrogen bonding. As seen in Table III, the CN force constants change very little, the bound CN values increasing by only about 1% for both dimer and trimer compared to the free CN group. The actual magnitudes of these changes are rather sensitive to the details of the particular force field chosen and so are not well determined. In contrast, the force constant for the CH bond involved in hydrogen bonding is significantly altered, a 6% decrease occurring for the dimer. An even greater drop of 11% is seen for the central CH bond of the trimer, implying that the second hydrogen bond is stronger than the first. This is not surprising since the (ΔE) per hydrogen bond is much greater for the trimer (3.8 kcal/mol) than for the dimer (2.69 kcal/mol).⁵³ The very low force constant for the central CH bond suggests a flow of charge in both directions from this bond, a process that might be favored by the pi network of a linear structure.

C. Spectra of higher polymers

The CARS spectra show a steady progression to lower frequency for all bands as the size of the complex increases. For expansions in which aggregation is extensive, a single, broad polymer feature dominates each spectral region, at frequencies which are essentially the same as those of the solid. While the CARS data afford no way of determining the sizes of the aggregates formed, most evidence points to small polymer sizes. In a separate mass spectral study to be described elsewhere⁵⁴ we have examined the size distributions in HCN and HCN/Ar expansions at $X/D = \infty$. As a typical example, for a 1:1 HCN/Ar expansion from $P_0 = 1.3$ atm we observe mass spectral signals of n -mers decreasing in the proportion 21:8:7:3:1 as n increases from 1 to 5. Questions do exist about the meaning of such intensities because of possible ionization fragmentation and, certainly, the conditions in these experiments are not identical to those used in the CARS apparatus. Nonetheless, a rapid falloff in concentration with cluster size is indicated. Similar observations have been made in mass spectrometric studies of water clusters⁵⁵ where the decay appears to be exponential with n for $n = 1$ to 40. These observations, coupled with the fact that we see the "polymer" band arise when the monomer, dimer, and trimer bands all have substantial intensity (see Figs. 13

and 14), indicate that the polymer band is characteristic of aggregates of the order of $n \sim 10$.

It is interesting to speculate about the nature of such small clusters. The fact that the frequencies we observe are very similar to those of the bulk solid and do not match the liquid frequencies (see Figs. 13, 15, and 16) suggests a solid-like packing. By solid-like we mean the strong preference for orderly linear hydrogen bonded chains. In the solid the hydrogen bond length is slightly smaller (2.18)³⁰ than the 2.22 Å value found in the gas phase dimer, so the shift of the polymer stretch to lower frequencies is indicative of similarly shorter, stronger hydrogen bonds. Finally, we do not mean to imply that the higher n -mers have the structure of one-dimensional chains. Clearly beyond a certain small number of units, say $n = 6$ or so, the dipole-dipole and dispersion interactions will eventually favor a structure having two or more parallel chains as opposed to one longer chain. However, we expect the linearity of chains to be strongly preferred over a random arrangement more characteristic of liquid type packing.

D. Line shape considerations

Much recent attention has been focused on the origin of vibrational linewidths for van der Waals and hydrogen bonded complexes, and it is appropriate to consider the present data (Table I) in this regard. The observed CARS linewidths are far in excess of the Doppler limit and can be either homogeneous, due to lifetime and dephasing effects, or inhomogeneous, due to the presence of multiple species, unresolved rotational fine structure, or the presence of combinations and hot bands with "intermolecular" modes. We cannot distinguish between homogeneous and inhomogeneous broadening in these experiments, but we can still eliminate some of the above mechanisms.

Rotational fine structure cannot be the main determinant of the observed linewidths. The sharpest Raman lines are the ν_1 modes of the HCN dimer and trimer, both of which show a FWHM = 2.6 cm^{-1} . Even here, the linewidths are much greater than expected on the basis of rotational structure alone. For example, if $\alpha/B_0 = +0.25\%$, as was estimated for the IR-active ν_1 dimer mode, the calculated CARS Q branch width due to rotational structure would be only 0.2 cm^{-1} (at 150 K). All of the observed widths are at least an order of magnitude larger than this.

We can reject the possibility that the observed dimer linewidths could be due to more than one species contributing to a given band. In expansions with mostly trimer and higher aggregates, little intensity contribution is seen in the dimer region. Thus, in Fig. 13 for example, the single, symmetric aggregate band produced in neat expansions of HCN can be attributed solely to the dimer. Similar considerations argue that the widths of the DCN CN and HCN CH dimer bands are also not due to contributions from higher aggregates.

We are thus led to consider lifetime effects and broadening due to transitions involving low frequency hydrogen bonding modes. The rate at which vibrational energy initially pumped into a high frequency mode of an isolated hydro-

gen bonded molecule redistributes among other coordinates is quite variable. In methanol dimer, the C–O stretching mode ($\sim 1050\text{ cm}^{-1}$) has a homogeneous linewidth of 13.8 cm^{-1} implying an extremely short lifetime for the C–O excitation (0.4 ps).¹³ In other cases such as $(\text{HF})_2$ the linewidths are quite narrow and lifetimes are greater by 5 orders of magnitude.⁷ This range of behavior has yet to be reconciled within the context of a theoretical picture. We only note here that, if our observed linewidths are homogeneous, they would imply lifetimes of $\sim 1\text{ ps}$ for the CN stretches in $(\text{HCN})_2$ dimer (and trimer), $\sim 0.3\text{ ps}$ for these modes in the $(\text{DCN})_2$, and $\sim 0.05\text{ ps}$ for the dimer CH stretch. It would be interesting to examine these modes using time domain coherent Raman spectroscopy⁵⁶ since the decay of the time delayed CARS signal would provide a sensitive measure of fast dephasing times.

Although lifetime effects may be present, it seems more likely that the observed widths arise from simple combinations of the CH and CN stretches with the low frequency stretching and bending modes of the hydrogen bond. In this picture, the anharmonic nature of the hydrogen bond potential gives “Franck–Condon” type vibrational progressions of the sort $\nu_{\text{AH}} + n\nu_{\text{HB}}$. Such a mechanism is known to be a major factor in producing the very broad A–H stretches in hydrogen bonded species^{4–6} and it, plus hot band transitions, could well account for the $\sim 60\text{ cm}^{-1}$ width we observe for the CH stretch of $(\text{HCN})_2$. A key feature of this model is the strength of coupling between the CH and CN bonds with the hydrogen bond, coupling reflected in both the monomer–dimer shifts and the widths of the dimer bands. It is not surprising that this interaction is smallest for the CN stretches in HCN thus making these the narrowest bands. The greater width of the ν_1 mode for DCN---DCN (11 vs 2.6 cm^{-1} for HCN---HCN) is consistent with the greater extent of mixing with the CD stretch which couples strongly to the hydrogen bond. We note that the same line of reasoning could also be invoked to explain the differences in lifetimes among the various modes if we attributed the widths to lifetime broadening. The distinction between these two viewpoints is of interest but must await further study of the homogeneous–inhomogeneous character of such hydrogen bonded transitions.

V. SUMMARY

The results obtained from infrared and PARS studies of static samples and from CARS spectroscopy in supersonic expansions allow us to make a number of observations concerning the nature of HCN complexes.

Our observations for the HCN dimer are completely consistent with the linear structure determined in microwave studies. The small positive vibration-rotation constant (α) determined for ν_1 indicates a small expansion of the molecule on excitation of the CN mode, a contrast to the larger contractions noted by others when the AH stretch is excited.^{35,36} The observed frequencies, and the force constants derived from them, show that very little perturbation of the CN bonds results from hydrogen bonding, consistent with results of *ab initio* calculations.^{57–60} As expected, the bonded CH stretch is much more affected. The 6% change in diag-

onal force constant and the dipole derivative increase implied by the 30-fold IR intensity enhancement of ν_1 are indicative of a substantial perturbation of this CH bond.

One of the most interesting aspects of the present work is the identification of the HCN trimer. The rotational envelope observed for the IR ν_1 trimer mode provides convincing evidence for a linear structure. To our knowledge, this is the most direct evidence for the structure of any gas-phase trimer yet observed. Other, less direct, vibrational predissociation results on $(\text{HF})_3$ ⁶¹ and $(\text{H}_2\text{O})_3$ ⁶² and their higher polymers, as well as electric deflection studies of a number of species⁶³ all point to cyclic structures for small n -mers with $n > 3$. HCN is somewhat unique in that the electron donating group is an sp hybridized lone pair. For a cyclic geometry, the s orbital of the hydrogen atom would have poorer overlap with such a lone pair and it is reasonable that the linear trimer should be preferred, even at the expense of one extra (but weaker) hydrogen bond.

All evidence indicates that the hydrogen bonds are stronger in the trimer than in the dimer. The CH frequency shifts of the trimer are larger, approaching those of solid HCN where the hydrogen bond lengths are significantly shorter than the gas phase dimer value. The trimer hydrogen bond energy is 3.8 kcal/mol per bond vs 2.7 kcal/mol in the dimer.⁵³ Finally, the IR ν_1 intensity enhancement relative to the monomer is much greater in the trimer (~ 500) than in the dimer (~ 30), indicating a greater electronic change in the CH bond. The trimer enhancement factor is very similar to the corresponding solid/gas cross section ratio of ~ 490 ,⁶⁴ suggesting a similarity to the solid.

We have little specific information concerning n -mers higher than the trimer except that all further species seem to have frequencies very near the solid state values. We conjecture that this is due to the presence of well-ordered linear arrangements in small clusters similar to the solid packing.

Our results point to the need for further work on HCN complexes. The linear HCN trimer should have a large dipole moment and thus be amenable to microwave study. Observation of even larger complexes, which we predict may be polar, might be possible. The bond lengths derived from such studies would be quite interesting in defining the hydrogen bonding potential energy surfaces of these model linear systems. In conjunction with this work, *ab initio* optimization of the trimer geometry would be enlightening.

Finally we note that the present study demonstrates the utility of CARS spectroscopy in supersonic expansions for studies of weakly bound complexes. Further research using CARS and other coherent Raman techniques should provide useful vibrational information to complement the valuable body of structural data recently obtained from microwave studies.

ACKNOWLEDGMENTS

This research has been supported by the AFOSR and the NSF. The authors thank Mr. George Pubanz and Dr. Gary Johnson for assistance with portions of this work. The pulsed nozzle and driving circuitry were based on designs by Dr. H. Selzle and JWN wishes to thank him and Professor E. Schlag for their hospitality during a sabbatical at the Techni-

cal University of Munich. JWN is also grateful to the Alexander von Humboldt Stiftung for a Senior Scientist Award during this period.

- ¹The *Hydrogen Bond*, edited by P. S. Schuster, G. Zundel, and C. Sandorfy (North-Holland, Amsterdam, 1976), Vols. I–III; M. D. Joesten and L. J. Schaad, *Hydrogen Bonding* (Marcel Dekker, New York, 1974); G. C. Pimentel and A. L. McClellan, *The Hydrogen Bond* (Freeman, San Francisco, 1960).
- ²T. R. Dyke, in *Topics in Current Chemistry*, edited by P. Schuster (Springer, New York, 1984), Vol. 120, p. 85.
- ³A. C. Legon, *J. Phys. Chem.* **87**, 2064 (1983); *Annu. Rev. Phys. Chem.* **34**, 275 (1983).
- ⁴C. Sandorfy, in *Topics in Current Chemistry*, edited by P. Schuster (Springer, New York, 1984), Vol. 120, p. 41.
- ⁵D. J. Millen, *J. Mol. Struct.* **100**, 351 (1983).
- ⁶J. C. Lassegues and J. Lascombe, in *Vibrational Spectra and Structure*, edited by J. R. Durig (Elsevier, New York, 1982) Vol. II, p. 51.
- ⁷A. S. Pine, W. J. Lafferty, and B. J. Howard, *J. Chem. Phys.* **81**, 2939 (1984); A. S. Pine, and W. J. Lafferty, *ibid.* **78**, 2154 (1983).
- ⁸N. Ohashi and A. S. Pine, *J. Chem. Phys.* **81**, 73 (1984).
- ⁹R. E. Miller and R. O. Watts, *Chem. Phys. Lett.* **105**, 409 (1984); R. E. Miller, P. F. Vohralik, and R. O. Watts, *J. Chem. Phys.* **80**, 5453 (1984).
- ¹⁰G. Hayman, J. Hodge, B. J. Howard, J. S. Muentzer, and T. R. Dyke (to be published).
- ¹¹R. J. Saykally and co-workers, presented at 32nd Western Spectroscopy Association Conference, 1985.
- ¹²W. Klemperer and co-workers, presented at 32nd Western Spectroscopy Association Conference, 1985.
- ¹³M. A. Hoffbauer, C. F. Giese, and W. R. Gentry, *J. Phys. Chem.* **88**, 181 (1984); M. J. Howard, S. Burdinski, C. F. Giese, and W. R. Gentry, *J. Chem. Phys.* **80**, 4137 (1984).
- ¹⁴G. A. Hopkins, M. Maroncelli, J. W. Nibler, and T. R. Dyke, *Chem. Phys. Lett.* **114**, 97 (1985).
- ¹⁵W. F. Giauque and R. A. Ruehrwein, *J. Am. Chem. Soc.* **61**, 2626 (1939).
- ¹⁶A. J. Fillery-Travis, A. C. Legon, L. C. Willoughby, and A. D. Buckingham, *Chem. Phys. Lett.* **102**, 126 (1983).
- ¹⁷E. J. Campbell and S. G. Kukolich, *Chem. Phys.* **76**, 225 (1983).
- ¹⁸L. W. Buxton, E. J. Campbell, and W. H. Flygare, *Chem. Phys.* **56**, 399 (1981).
- ¹⁹R. D. Brown, P. D. Godfrey, and D. A. Winkler, *J. Mol. Spectrosc.* **89**, 352 (1981).
- ²⁰A. C. Legon, D. J. Millen, and P. J. Mjoberg, *Chem. Phys. Lett.* **47**, 589 (1977).
- ²¹B. Walsh, A. J. Barnes, S. Suzuki, and W. J. Orville-Thomas, *J. Mol. Spectrosc.* **72**, 44 (1978).
- ²²J. Pacansky, *J. Phys. Chem.* **81**, 2240 (1977).
- ²³C. M. King and E. R. Nixon, *J. Chem. Phys.* **48**, 1685 (1968).
- ²⁴E. Knozinger and R. Wittenbeck, *Ber. Bunsenges, Phys. Chem.* **86**, 742 (1982).
- ²⁵H. D. Mettee, *J. Phys. Chem.* **77**, 1762 (1973).
- ²⁶W. J. Jones, R. M. Seel, and N. Sheppard, *Spectrochim. Acta Part A* **25**, 385 (1969).
- ²⁷I. R. Dagg, and H. W. Thompson, *Trans. Faraday Soc.* **52**, 455 (1956).
- ²⁸G. E. Hyde and D. F. Hornig, *J. Chem. Phys.* **20**, 647 (1952).
- ²⁹T. F. Lundeen, Ph. D. thesis, Oregon State University, 1984.
- ³⁰A useful summary of spectroscopic studies of HCN up to 1973 was given by B. M. Chadwick and H. G. M. Edwards, *Mol. Spectrosc.* **1**, 446 (1973).
- ³¹J. Bendtsen and H. G. M. Edwards, *J. Raman Spectrosc.* **2**, 407 (1974).
- ³²A. G. Maki and L. R. Blaine, *J. Mol. Spectrosc.* **12**, 45 (1964).
- ³³T. Nakagawa and Y. Morino, *Bull. Chem. Soc. Jpn.* **42**, 2212 (1969).
- ³⁴The uncertainties quoted for the IR and Raman cross sections arise from different sources. The large uncertainty in the IR values comes mainly from difficulty in measuring the intensity of ν_1 accurately due to the presence of interspersed lines of the $3\nu_2$ transition. The Raman uncertainty given here is the statistical error estimate from the least squares fit to Eq. (1). Also note that errors in σ_D/σ_M and σ_T/σ_M are highly correlated in both cases.
- ³⁵E. Kyro, P. Shoja-Chaghervand, K. McMillan, M. Eliades, D. Danzeiser, and W. J. Bevan, *J. Chem. Phys.* **79**, 78 (1983); E. Kyro, R. Warren, K. McMillan, E. Eliades, D. Danzeiser, P. Shoja-Chaghervand, S. G. Lieb, and J. W. Bevan, *ibid.* **78**, 5881 (1983).
- ³⁶R. K. Thomas, *Proc. R. Soc. London Ser. A* **344**, 579 (1975); **325**, 133 (1971); R. K. Thomas and H. Thompson, *ibid.* **316**, 303 (1970).
- ³⁷E. K. Gustafson, Ph. D. thesis, Stanford University 1983.
- ³⁸W. J. Dulmage and W. N. Lipscomb, *Acta Crystallogr.* **4**, 330 (1951).
- ³⁹See, for example, (a) D. Goulomb, R. E. Good, and R. F. Brown, *J. Chem. Phys.* **52**, 1545 (1970); (b) T. A. Milne, A. E. Vandegrift, and F. T. Greene, *ibid.* **52**, 1552 (1970).
- ⁴⁰Raman data for solid and liquid HCN and DCN are taken from Ref. 41. The frequency ranges shown in the figure refer in the liquid case to the FWHH of the Raman band at 261 K. In the solid there are two phases (I and II) which have slightly different Raman shifts and widths. Here we have shown the region demarked by the superposed FWHHs of both phases I (183 K) and II (78 K).
- ⁴¹M. Pezolet and R. Savoie, *Can. J. Chem.* **47**, 3041 (1969).
- ⁴²G. L. Johnson and L. Andrews, *J. Am. Chem. Soc.* **105**, 163 (1983).
- ⁴³R. M. Seel and N. Sheppard, *Spectrochim. Acta Part A* **25**, 1295 (1969).
- ⁴⁴D. H. Aue and M. T. Bowers, in *Gas Phase Ion Chemistry*, edited by M. T. Bowers (Academic, New York, 1979), Vol. 2, p. 1.
- ⁴⁵G. T. Fraser, K. R. Leopold, D. D. Nelson, Jr., A. Tung, and W. Klemperer, *J. Chem. Phys.* **80**, 3073 (1984).
- ⁴⁶A. J. Barnes, *J. Mol. Struct.* **100**, 259 (1983).
- ⁴⁷O. Schrems, H. M. Oberhoffer, and W. A. P. Luck, *J. Phys. Chem.* **88**, 4335 (1984).
- ⁴⁸These values are in good agreement with the recent theoretical predictions of P. Botschwina, *Chem. Phys.* **81**, 73 (1983).
- ⁴⁹J. E. Gready, G. B. Bacskay, and N. S. Hush, *Chem. Phys.* **31**, 467 (1978).
- ⁵⁰C. Perchard and J. P. Perchard, *J. Raman Spectrosc.* **7**, 173 (1978); J. Limiouzi, A. Burneau, and J. P. Perchard, *Chem. Phys. Lett.* **47**, 346 (1977).
- ⁵¹D. G. Rea, *J. Chem. Phys.* **33**, 1875 (1960).
- ⁵²B. A. Zilles and W. B. Person, *J. Chem. Phys.* **79**, 65 (1983).
- ⁵³These values were obtained from the ΔH values of Ref. 15 noting the difference between ΔE and ΔH : $\Delta E = \Delta H - \Delta nRT$.
- ⁵⁴T. R. Dyke (to be published).
- ⁵⁵D. Dreyfuss and H. Y. Wachman, *J. Chem. Phys.* **76**, 2031 (1982).
- ⁵⁶H. Graener, A. Laubereau, and J. W. Nibler, *Opt. Lett.* **9**, 165 (1984).
- ⁵⁷A. Karpfen, *Chem. Phys.* **79**, 211 (1983).
- ⁵⁸B. A. Pettitt, R. J. Boyd, and K. E. Edgcombe, *Chem. Phys. Lett.* **89**, 478 (1982).
- ⁵⁹S. Scheiner, *Theor. Chim. Acta (Berl.)* **57**, 71 (1980).
- ⁶⁰A. Johansson, P. Kollman, and S. Rothberg, *Theor. Chim. Acta (Berl.)* **26**, 97 (1972).
- ⁶¹J. M. Lisy, A. Tramer, M. F. Vernon, and Y. T. Lee, *J. Chem. Phys.* **75**, 4733 (1981).
- ⁶²M. F. Vernon, D. J. Krajnovich, H. S. Kwok, J. M. Lisy, Y. R. Shen, and Y. T. Lee, *J. Chem. Phys.* **77**, 47 (1982).
- ⁶³J. A. Odutola, R. Viswanathan, and T. R. Dyke, *J. Am. Chem. Soc.* **101**, 4787 (1979); T. R. Dyke and J. S. Muentzer, *J. Chem. Phys.* **57**, 5011 (1972).
- ⁶⁴H. B. Friedrich and P. F. Krause, *J. Chem. Phys.* **59**, 4942 (1973).